Columnar Mesomorphism from Hemi-Disklike Metallomesogens Derived from 2,6-Bis[3′,4′,5′-tri(alkoxy)phenyliminomethyl]pyridines (L): Crystal and Molecular Structures of [M(L)Cl_2] (M = Mn, Ni, Zn)

Francesca Morale,[b] Richard W. Date,[c] Daniel Guillon,[a] Duncan W. Bruce,[c] Rachel L. Finn,[b] Claire Wilson,[b] Alexander J. Blake,[b] Martin Schröder,[b] and Bertrand Donnio*[a]

Abstract: Four new series of non-disklike complexes of general formula [$MCl_2(L^n)$] based upon substituted 2,6-bis(3′,4′,5′-trialkoxyphenyliminomethyl)-pyridine ligands (L^n) and with M = Zn^{II}, Co^{II}, Mn^{II}, and Ni^{II} have been prepared and examined for liquid crystallinity. A complete analysis of the thermal behavior by polarized-light optical microscopy, differential scanning calorimetry, and small-angle X-ray scattering revealed a rich and varied mesomorphism. Moreover, the high thermal stability of the compounds leads to rather extended mesomorphic ranges. The nature and thermal stability of each mesophase depend on both the length of the six terminal alkoxy chains, n (n = 8, 10, 12, 14, 16), and on the metal ions. As demonstrated by small-angle X-ray diffraction experiments, the mesomorphism of these complexes is solely of the columnar type. One compound shows an oblique columnar phase, while most of them show a hexagonal columnar phase, Col_h, and several types of rectangular columnar phase, Col_r. X-ray single-crystal structures obtained for three methoxy derivatives confirm the 1:1 metal–ligand stoichiometry of the complexes, in which the metal is pentacoordinate with a distorted, trigonal bipyramidal geometry. The crystalline structures also reveal the existence of some columnar organization in the solid state, the columns resulting from an alternated stacking of the complexes in one direction. By combining these results with those obtained from dilatometry experiments, a model for the molecular organization within the mesophases is proposed in which an antiparallel arrangement of the metallomesogens is retained in the mesophase.

Keywords: coordination chemistry · liquid crystals · metallomesogens · tridentate ligands · X-ray diffraction

Introduction

Metallomesogens, liquid-crystalline metal complexes, continue to attract much attention, not only for the opportunities they offer for the design of new functional materials, but also for their potential to expand the range of technological applications and properties exhibited by anisotropic fluids by incorporating specific properties of metal ions.[1] Moreover, due to the various oxidation states and the large variety of coordination geometries available,[2] metal ions offer many possibilities as building blocks for unique molecular structures when associated with suitably designed ligands. This, in turn, may lead to new types of molecular organization and potentially to new mesophase symmetries. Another important aspect of the incorporation of metal ions resides in the induction, modification, or enhancement of the mesomorphism of the free parent ligands. New rational design methodologies to produce organized molecular assemblies with specific interactions (e.g., dipolar and metal–ligand interactions) are, therefore, not only important but also challenging. Such systematic studies will give a better understanding of the role of these interactions, and help identify specific structure–property relationships for the purpose of the design of specific materials.

The present work relates to the design of routes to metallomesogens capable of generating columnar structures, such systems finding potential technological applications in

[a] Dr. B. Donnio, Dr. D. Guillon
Institut de Physique et Chimie des Matériaux de Strasbourg (IPCMS)
Groupe des Matériaux Organiques (GMO)
UMR 7504 (CNRS-ULP), 23 rue du Loess, BP 43
67034 Strasbourg Cedex 2 (France)
Fax: (+33) 388-10-72-46
E-mail: bdonnio@ipcms.u-strasbg.fr

[b] Dr. F. Morale, Dr. R. L. Finn, Dr. C. Wilson, Dr. A. J. Blake, Prof. M. Schröder
School of Chemistry, University of Nottingham
University Park, Nottingham NG7 2RD (UK)

[c] Dr. R. W. Date, Prof. D. W. Bruce
School of Chemistry, University of Exeter
Stocker Road, Exeter EX4 4QD (UK)

Supporting information for this article is available on the WWW under http://www.chemeurj.org/ or from the author.

DOI: 10.1002/chem.200204578

the fields of electronic and ionic transport or photonics.[3] One such development is illustrated through an original concept initiated separately by Serrano[4] and Swager[5] for the design of new columnar arrangements of metallomesogens based on specific molecular interactions. This approach, formerly known as the *complementary molecular shape* approach,[5] generates time-averaged correlations between hemi-disk-shaped metal complexes, for example, antiparallel correlation between nearest neighbor molecules, to produce columns that are able to self-organize further into mesophases (Figure 1). This time-averaged alternating stacking can be stabilized by metal–metal, metal–ligand, and/or dipolar interactions, but, most importantly, by the steric and topological constraints imposed by the peripheral chain structure. Thus, the cross section of the hard columnar cores adopts the shape of a disk or ellipse with the symmetry of the mesophase depending on both the molecular structure and the type of interactions involved. These materials are of course fluids, and Figure 1 is a schematic representation of such time-averaged arrangements.

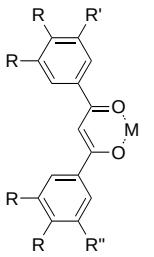

1a: M=Tl; R=$OC_{10}H_{21}$; R′=R″=H
1b: M=Tl; R=R′=$OC_{10}H_{21}$; R″=H
2: M=$Rh(CO)_2$, $Ir(CO)_2$;
R=R′=R″OC_nH_{2n+1};*n*=4,6,8,10,12,14,16,18

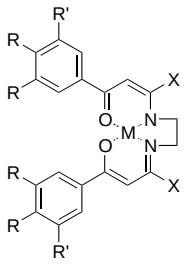

3a: X=CH_3; M=Ni, Cu, Pd, VO; R=R′=OC_nH_{2n+1}; *n*=10,12,16
3b: X=H; M=Ni, Cu; R=R′=OC_nH_{2n+1}; *n*=10,12,14,16,18
3c: X=H; M=Ni, Cu, Co, VO; R=OC_nH_{2n+1}; R′=H; *n*=6,8,10,12,14,16

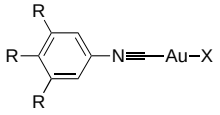

4: X= Cl, Br, I; R=OC_nH_{2n+1}; *n*=4,6,810

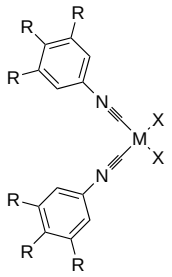

5: M=Pt, Pd; X=Cl, Br
R=OC_nH_{2n+1}; *n*=4,6,8,10

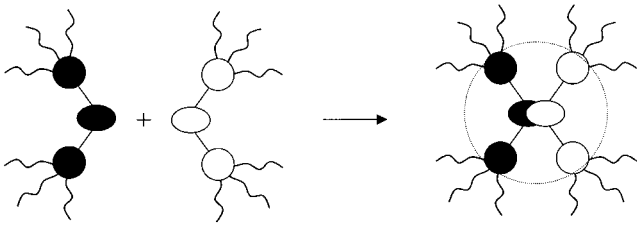

Figure 1. Illustration of the antiparallel mode of the molecular arrangement that forms columnar mesophases in time-averaged disklike structures from non-disklike metallomesogens.

This concept, essentially developed by Swager, has been applied successfully to the induction of columnar mesophases in a variety of hemi-disk-like complexes such as 1:1 metal–ligand complexes (**1**–**4**)[4, 5b, 6–8] and a few 1:2 metal–ligand complexes (**5**),[9] as well as in more sophisticated homo- and heteronuclear bimetallic molecular structures.[5a, 10] In these examples, intermolecular recognition may take place by means of direct metal–metal interactions (**1**), weak metal–metal interactions (**2**, **3a**, **4**, and **5**), metal–ligand mediated interactions (**3**), dipolar interactions (**2**, **3**, **4**, and **5**), or steric effects. For example, in **1**–**5**, the number the aliphatic chains imposes important volume constraints that are believed to be essential driving forces in columnar mesophase stabilization. Note that the columnar structures derived from such molecular arrangements have been described as columnar *anti-phases*,[10] a slightly misleading term that will not be used hereinafter to avoid confusion.

Metal complexes derived from Schiff-base ligands feature among the earliest and most widely studied class of metallomesogens.[1, 11] In general, the advantages of incorporating an imine functionality lie in the versatility, structural variety, and ease of preparation and derivatization of such groups. Tridentate Schiff-base ligands obtained by the condensation of 2,6-disubstituted pyridines (dialdehydes or diketones) and aromatic amines have been investigated since the early 1970's,[12] because of the strong coordinating ability of the *N,N′,N′* donor set. A range of late first-row transition-metal complexes of such bis(phenylimino)pyridine ligands has been synthesized and fully characterized,[12, 13] and, more recently, some have attracted attention as high-activity olefin polymerization catalysts[14] and as general molecular templates for supramolecular systems.[15] Transition-metal ions with such ligands therefore tend to form either mono- or bis-ligand complexes of type $[M(L)]^{x+}$ or $[M(L)_2]^{x+}$, respectively.

To date, very few metallomesogens derived from 2,6-bis(phenyliminomethyl)pyridine have been reported. Dalcanale et al. carried out a systematic study[16] on mono-ligand Ni^{II} and Pd^{II} complexes based on substituted 2,6-bis(phenylhydrazone)pyridines (Figure 2) as potential columnar metallomesogens. One complex [Ni(L)] showed a mesophase (unidentified) during the first heating only, and converted upon further heating into the more stable, but nonmesogenic, paramagnetic discrete dimeric form. Ziessel and co-workers[17] have illustrated the versatility of multitopic ligands derived from 2,6-diiminopyridines as building blocks for the construction of unusual architectures, such as metallohelicates. Thus, the formation of suitable ligands by the attachment of groups bearing terminal alkoxy chains to 2,6-diiminopyridines (Figure 2) and their subsequent coordination to Cu^{I} afforded tetrahedral metallomesogens $[Cu(L)_2][BF_4]$ showing a columnar hexagonal mesophase.[18]

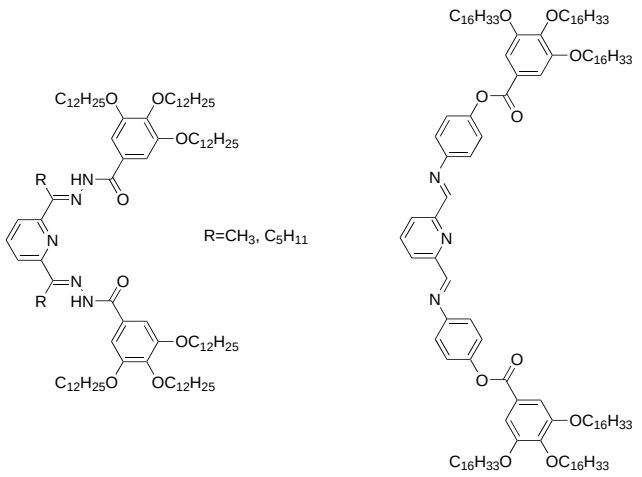

Figure 2. Dalcanale's 2,6-bis[(3′,4′,5′-trialkoxy)phenylhydrazone]pyridine[16] (left) and the Ziessel's elongated 2,6-bisiminepyridine[17] (right) as potential ligands for metallomesogens.

These encouraging results prompted us to synthesize some novel hemi-disk complexes of the type $[MCl_2(L^n)]$ to determine whether columnar mesophases could be induced in a similar manner. The ligand adopted for the current investigation is a derivatized 2,6-bis(phenyliminomethyl)pyridine [L^n = 2,6-bis(3′,4′,5′-trialkoxyphenyliminomethyl)pyridine], and the metal ions belong to the first transition series [Zn^{II} (d^{10}), Co^{II} (d^7), Mn^{II} (d^5), and Ni^{II} (d^8)]. For each metal, a series of complexes was obtained by using ligands with different alkoxy chain lengths ($n = 8, 10, 12, 14, 16$). We report herein the synthesis and characterization of four series of novel neutral metallomesogens, the X-ray single crystal structures of Mn^{II}, Ni^{II}, and Zn^{II} derivatives, and the evaluation of the mesomorphic behavior of these species. A model for the molecular organization within the mesophases is also proposed.

Results and Discussion

Synthesis: The coordination complexes (Scheme 1) were prepared by the template Schiff-base condensation of 2,6-pyridinedicarboxaldehyde with two molar equivalents of the appropriate 3,4,5-trialkoxyaniline in the presence of one molar equivalent of MCl_2. The reaction conditions and workup procedures vary only slightly for each series and consist of heating a solution of MCl_2, 2,6-pyridinedicarboxaldehyde, and the 3,4,5-trialkoxyaniline under reflux in $CHCl_3$/EtOH for 20 h in all cases except for the Mn^{II} complexes, which were prepared by stirring for the same time but at room temperature. The complexes were obtained as precipitates either by slow evaporation of the solvent or, in the case of the Ni^{II} complexes, by reducing the volume of the reaction mixture. The 3,4,5-trialkoxyanilines were synthesized by following a method described previously.[19]

In addition, two of the free ligands, L^1 and L^{16}, were also prepared to allow identification of the complexes under study by comparative IR, UV-visible and NMR spectroscopy, and, in the former case, to prepare metal complexes which yielded single crystals.

Characterization of complexes: The complexes were characterized systematically by IR and UV-visible spectroscopy, mass spectrometry, and elemental analysis as well as by ^1H and ^{13}C NMR spectroscopy for the diamagnetic zinc(II) complexes. The IR spectra of the products and free ligands show the absence of the amine and carbonyl absorptions associated with the starting aniline and dialdehyde materials. The medium-intensity band at around 1590 cm^{-1}, assigned to the C=N stretching vibration, confirms the formation of the Schiff-base product and is thought to occur at relatively low frequency, because of the highly conjugated nature of the ligand system; typical imine stretches were found between 1690 and 1640 cm^{-1}. Interestingly, only small shifts in the frequency of the C=N absorption was detected upon complexation of the ligand.

The UV-visible spectra of the free ligands L^1 and L^{16} display two absorption maxima, near 240 and 360 nm. The electronic ligand transition near 240 nm remains effectively unchanged in shape, intensity ($\varepsilon = 2.4 - 3.7 \times 10^4\ mol^{-1}\,dm^3\,cm^{-1}$) and position in the complexes, which also show at least two other bands of lower intensity, centered around 286 – 301 nm and 406 – 441 nm. Another charge-transfer absorption appears in the spectra of the nickel(II) compounds between 383 and 394 nm. The lowest frequency bands impede observation of the d – d transitions expected in the 400 nm region of the spectrum.

Comparative analysis by ^1H NMR spectroscopy shows that the signal arising from the two equivalent imine protons of the free ligands L^1 and L^{16}, at approximately $\delta = 8.7$ ppm undergoes a slight down-field shift of around 0.1 ppm upon complexation to $ZnCl_2$, the retained equivalence confirming the formation of a symmetrical compound. More significant changes are observed for the pyridine and aromatic ring protons. In the region $\delta = 8.2 - 7.9$ ppm a characteristic pattern is observed for the 2,6-disubstituted pyridine ring of the free ligands, with the doublet resonance of the pyridine protons *meta* to the ring nitrogen atom observed downfield with respect to the triplet assigned to the *para* proton. This pattern is reversed in the spectra of the complexes, in which the triplet is found downfield with respect to the doublet, in the region

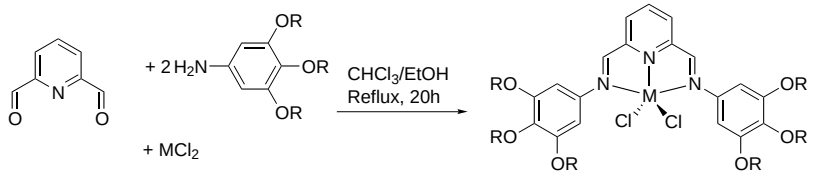

$[MCl_2(L^n)]$
M = Zn, Co, Mn, Ni
L^n : R = C_nH_{2n+1} ; n = 1, 8, 10, 12, 14, 16

Scheme 1. Template synthesis of the metal dichloride complexes of 2,6-bis-[(3′,4′,5′-trialkoxy)phenylimine-methyl]pyridine, $[MCl_2(L^n)]$.

$\delta = 7.9 - 7.7$ ppm. Following complexation, the aromatic protons of the lateral phenyl substituents shift remarkably downfield, by approximately 0.7 ppm, from the typical value of $\delta = 6.6$ ppm observed in the free ligands. No significant changes are observed in the aliphatic region on complex formation. Assignments by ^{13}C NMR spectroscopy were made by means of C–H correlation experiments. Microanalysis and mass spectrometry provided evidence of the formation of the 1:1 metal–ligand complexes, and excluded the formation of six-coordinate 1:2 metal–ligand products of type $[M(L)_2]^{2+}$. Conductivity measurements in chloroform for the complexes $[MCl_2(L^{16})]$ were undertaken in order to establish the role of the Cl^- ions in solution; the low conductivity suggested the direct binding of both Cl^- ions to the metal.

Crystal and molecular structure of the model compounds $[MCl_2(L^1)]$ (M = Mn, Ni, Zn): In order to better determine how these complexes might arrange themselves spatially, X-ray single-crystal structures were obtained for the complexes of general formula $[MCl_2(L^1)]$ ($M = Mn^{II}$, Ni^{II}, Zn^{II}); no suitable crystals were obtained with cobalt. The results will be discussed together as the structures identified are geometrically quite similar (Figure 3). Note that these short-chain complexes were chosen as it did not prove possible to obtain diffraction-quality crystals of any of the longer-chain homologues.

Yellow, lath-like crystals of $[MnCl_2(L^1)] \cdot 0.5\,PhCN$ were obtained by diffusion of pentane into a solution of the complex in benzonitrile. Orange columnar crystals of $[ZnCl_2(L^1)] \cdot 0.5\,PhCN$ were grown by layering a solution of the ligand in PhCN with a solution of $ZnCl_2$ in EtOH (1:1). Two different solvates of $[NiCl_2(L^1)]$ with nitrobenzene and benzonitrile ($[NiCl_2(L^1)] \cdot PhNO_2$ and $[NiCl_2(L^1)] \cdot PhCN$) were obtained as orange tablets by diffusion of *n*-pentane into a solution of the product in nitrobenzene and from a layered PhCN/EtOH (1:1) solution of the ligand and $NiCl_2 \cdot 6\,H_2O$. Crystallographic data for these compounds are listed in Table 1.

Table 2 presents selected bond lengths and the values for the mean deviation of the metal from the diiminopyridyl plane. Selected angles are given in Table 3 together with selected torsion angles of the lateral phenyl rings and the mean deviation of the atoms forming the ligand plane.

All structures consist of a neutral complex of general formula $[MCl_2(L^1)]$ and possess approximate, noncrystallographic C_2 symmetry about a plane that bisects the central pyridine ring and contains the metal center and the two Cl^- ions (Figure 3). The metal ions are in a distorted trigonal bipyramidal environment defined by the planar tridentate N-donor set of the ligand and the two Cl^- ions. The pyridyl nitrogen (N_{py}) and the two Cl^- ligands form the equatorial or trigonal plane, with the two imine nitrogens (N_{im}) providing the axial donors. As a consequence of satisfying the tridentate chelate constraints of the ligand, the $M-N_{im}$ bond lengths are essentially identical and noticeably longer than the $M-N_{py}$ bond length. The distorted axial and bite angles subtended by these atoms (N_{im}-M-N_{im} and N_{im}-M-N_{py}) are much reduced from 180° and 90°, respectively. Sterically, the Mn^{II} compound displays the most constrained structure due to longer bond lengths, as might be expected for a high-spin d^5 ion of larger ionic radius. The axial angle N(2)-Mn-N(3) is thus reduced to 143° (versus 148 and 155° for $[ZnCl_2(L^1)]$ and $[NiCl_2(L^1)]$, respectively) and the $M-N_{pyridyl}$ distance is closer to the $M-N_{imine}$ bond lengths than in any of the other complexes of the type $[MCl_2(L^1)]$ considered ($M = Ni^{II}$ and Zn^{II}).

Deviation from planarity upon coordination is induced for the two five-membered chelate rings of the diiminepyridyl moiety by slight torsions (2–3°) about the two $C_{py}-C_{im}$ bonds. The diimine ligand adopts an *E*–*E* configuration, as expected on the basis of steric considerations.

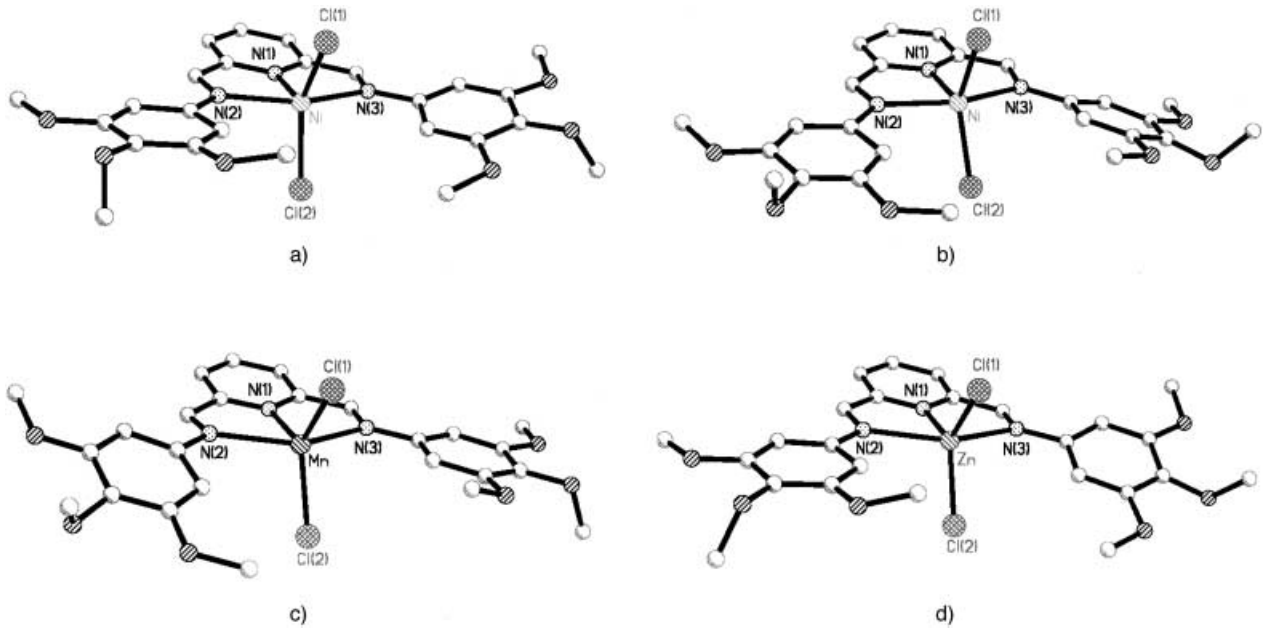

Figure 3. Molecular structures of a) $[NiCl_2(L^1)] \cdot PhNO_2$, b) $[NiCl_2(L^1)] \cdot PhCN$, c) $[MnCl_2(L^1)] \cdot 0.5\,PhCN$, and d) $[ZnCl_2(L^1)] \cdot 0.5\,PhCN$, with part of the numbering scheme adopted. Solvent molecules and hydrogen atoms have been omitted for clarity.

Table 1. Selected crystallographic data for $[MnCl_2(L^1)]\cdot 0.5\,PhCN$, $[NiCl_2(L^1)]\cdot PhCN$, $[NiCl_2(L^1)]\cdot PhNO_2$, and $[ZnCl_2(L^1)]\cdot 0.5\,PhCN$.

	$[MnCl_2(L^1)]\cdot 0.5\,PhCN$	$[NiCl_2(L^1)]\cdot PhCN$	$[NiCl_2(L^1)]\cdot PhNO_2$	$[ZnCl_2(L^1)]\cdot 0.5\,PhCN$
formula	$C_{28.5}H_{29.5}Cl_2MnN_{3.5}O_6$	$C_{32}H_{32}Cl_2N_4NiO_6$	$C_{31}H_{32}Cl_2N_4NiO_8$	$C_{28.5}H_{29.5}Cl_2N_{3.5}O_6Zn$
M_r	642.90	698.23	718.22	653.33
crystal system	triclinic	triclinic	triclinic	triclinic
space group	$P\bar{1}$	$P\bar{1}$	$P\bar{1}$	$P\bar{1}$
color	yellow	orange	orange	orange
a [Å]	10.982(10)	9.220(5)	9.556(3)	10.9365(9)
b [Å]	12.052(11)	12.417(6)	12.465(4)	12.034(1)
c [Å]	12.736(11)	14.341(7)	14.348(4)	12.715(1)
α [°]	103.61(2)	84.927(9)	90.247(5)	103.707(1)
β [°]	100.40(2)	89.485(9)	94.352(5)	99.915(1)
γ [°]	111.56(2)	80.048(9)	99.942(5)	111.021(1)
V [Å^3]	1456(4)	1610.8(13)	1678.3(9)	1455.3(4)
T [K]	150(2)	150(2)	150(2)	150(2)
Z	2	2	2	2
reflections collected	7877	13045	14416	13000
unique reflections[a]	5704 (4295)	7152 (3176)	7416 (3041)	6612 (5077)
R(int)	0.025	0.0112	0.129	0.024
parameters	366	406	415	366
$R1$ [$I > 2\sigma(I)$]	0.0805	0.0853	0.0872	0.0411
$wR2$ (all data)	0.3962	0.2591	0.2644	0.1158
GOF	1.029	0.992	0.975	1.021

[a] [$I > 2\sigma(I)$].

Table 2. Selected bond lengths [Å] and mean deviations (dev.) [Å] of the metal atom from the N_3 ligand plane for $[MCl_2(L^1)]$ complexes.

	M–N(1)[a]	M–N(2)[a]	M–N(3)[a]	M–Cl(1)	M–Cl(2)	dev.
$[MnCl_2(L^1)]\cdot 0.5\,PhCN$	2.169(5)	2.350(5)	2.353(5)	2.357(2)	2.338(3)	0.0253
$[NiCl_2(L^1)]\cdot PhCN$	1.943(6)	2.151(6)	2.153(6)	2.262(2)	2.260(2)	0.0560
$[NiCl_2(L^1)]\cdot PhNO_2$	1.948(7)	2.177(6)	2.191(6)	2.295(2)	2.288(2)	0.0517
$[ZnCl_2(L^1)]\cdot 0.5\,PhCN$	2.051 (2)	2.324(2)	2.328(2)	2.2549(8)	2.2385(8)	0.0186

[a] $N(1) = N_{py}$; $N(2)$, $N(3) = N_{im}$.

Table 3. Selected angles [°] for complexes $[MCl_2(L^1)]$, characterizing the coordination environment and the twist (torsion) of the two lateral phenyl rings with respect to the diiminopyridyl ligand plane. The mean deviation [Å] from planarity of the atoms defining this plane is also reported.

	$[MnCl_2(L^1)]\cdot 0.5\,PhCN$	$[NiCl_2(L^1)]\cdot PhCN$	$[NiCl_2(L^1)]\cdot PhNO_2$	$[ZnCl_2(L^1)]\cdot 0.5\,PhCN$
bite angles				
N(1)-M-N(2)	71.3(2)	77.4(2)	78.0(2)	74.08(8)
N(1)-M-N(3)	71.7 (2)	77.2(2)	77.0(2)	74.31(8)
axial angle				
N(2)-M-N(3)	143.0(2)	154.5(2)	154.9(3)	148.36(8)
trigonal angles				
N(1)-M-Cl(1)	120.64(14)	108.1(2)	114.9(2)	120.32(7)
N(1)-M-Cl(2)	122.37(14)	121.7(2)	111.4(2)	121.74(7)
Cl(1)-M-Cl(2)	116.98(9)	130.16(8)	133.69(9)	117.93
torsion angles[a]	20.1, 3.4	3.4, 13.2	2.3, 11.1	5.3, 18.6
N_3 plane[b] (mean deviation)	0.0194	0.0167	0.0144	0.0175

[a] The torsion angles measured are C(6)-N(2)-C(10)-C(11) and C(7)-N(3)-C(20)-C(21). [b] The atoms defining this plane are C(1), C(2), C(3), C(4), C(5), C(6), C(7), N(1), N(2), and N(3).

Difficulties in distinguishing between trigonal-bipyramidal and square-pyramidal stereochemistries arise in distorted systems, and analyses reported by other researchers[14a,c, 20, 21] outline the boundary geometries for compounds of this class. The criteria drawn up include deviation of the metal from the N_3 ligand plane and the asymmetry in the M–Cl linkages. Out-of-plane positioning of the central metal (by up to 0.6 Å) and lengthening of one of the two M–Cl bonds (by as much as 0.03 – 0.05 Å), which would distinguish the apical chloro ligand from its basal counterpart, indicate departure from trigonal-bipyramidal towards square-pyramidal geometry. On the basis of such considerations, a pseudo-trigonal-bipyramidal stereochemistry was assigned to all complexes of the type $[MCl_2(L^1)]$.

In all the structures, the two lateral phenyl rings present on the imine moieties do not lie perfectly in the coordination plane of the ligand backbone, exhibiting inequivalent torsion angles of about 11 – 20° and 3 – 7°. Overall, such degrees of twisting are quite small relative to those observed in numerous related structures,[13d, 14a,c, 20, 21] and the ligand portion of these $[MCl_2(L^1)]$ complexes can be regarded as almost planar. This can perhaps be attributed to the absence both of methyl groups at the imine carbon and of *ortho* substituents on the phenyl rings. Indeed, the structure of the zinc(II)

complex with the aldimine ligand derivative bearing *para*-OH groups on the rings, reported by Busch and co-workers,[15] also shows near coplanarity of the ligand framework. The planarity of the complexes will be of relevance to their supramolecular organization, as discussed below.

Of particular interest to the present study is the molecular packing mode of the complexes $[MCl_2(L^1)]$. The way in which these units are arranged with respect to each other in the solid state assists the understanding of the columnar organization found for their long-chain analogues in the liquid crystalline state. These packing modalities will be discussed only with reference to the complex $[NiCl_2(L^1)]\cdot PhCN$, as they are typical for all four compounds of the type $[MCl_2(L^1)]$ examined (Figure 4).

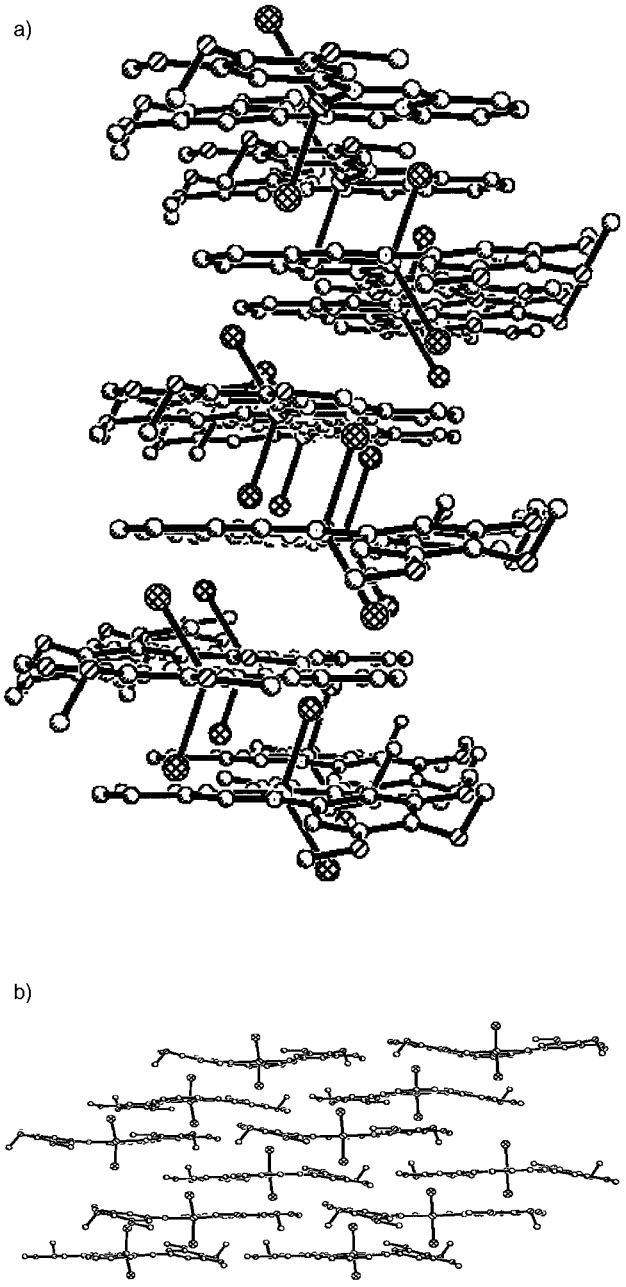

Figure 4. Two complementary views of the packing of $[NiCl_2(L^1)]\cdot PhCN$, showing a) how the molecules in adjacent layers are related through inversion centres and b) a view parallel to the layers.

In terms of Ni···Ni separations, the nearest neighbors form a steplike arrangement of molecules (Figure 4a), whereby adjacent molecules are related by an inversion center. There are two alternating Ni···Ni separations of 6.502 and 6.766 Å and this 'chain' of atoms runs parallel to the *b*-axis. As shown in Figure 4b, these step-like arrangements stack on one another along the *a*-axis direction (the next nearest Ni···Ni distance is 9.22 Å) and are separated by layers of solvent molecules (omitted from this picture). The molecular units do not stack directly above one another in a head-to-head manner, but adopt a head-to-tail configuration with the pyridine rings lying over the phenyl rings. It is the overall near planarity exhibited by the complexes that allows these molecules to arrange themselves linearly in successive parallel layers. The main features of the packing diagrams for the other three complexes are essentially the same.

The molecular packing mode observed is reminiscent of pre-existing columns. Indeed, the complexes $[MCl_2(L^1)]$ pack to form columns parallel to the crystallographic *c*-axis with molecules arranged in a head-to-tail fashion, that is the nearest-neighbor molecules are rotated by 180° to give an overall disklike topology with an average distance between two neighboring metal centers of approximately 6.5–7 Å. This crystalline structure can, therefore, be regarded as related to the columnar mesophases present above the crystal phase, as described below. Note that several other crystalline structures of related bis(imine)pyridine coordinated with MCl_2 units differing in the substitution patterns of the terminal phenyl rings and on the metal centers have been studied, and all of them display the same structural features.[12, 13, 15] Therefore, it seems that the trigonal bipyramidal geometry and subsequent packing into a pseudocolumnar arrangement are characteristic of such complexes in the crystalline state;[14a, 15] analogous structural characteristics are likely to be extended to the rest of the series of complexes described.

Liquid-crystalline properties: The free ligands L^1 and L^{16} are not mesomorphic. Given the structure of the ligand (bent shape, small anisotropy, small aspect ratio) similar behavior is also expected for the other ligands. However, the subsequent coordination of the ligands L^8, L^{10}, L^{12}, L^{14}, and L^{16} to the various MCl_2 fragments confers liquid-crystalline properties on the resulting complexes, possibly by fixing the ligand into an optimum conformation to allow mesophases to form. The mesophases exhibited by these materials exist over large temperature ranges, illustrating the mesophase induction and stabilization upon complexation referred to in the introduction.

Mesomorphism by optical microscopy and differential scanning calorimetry: The above complexes were investigated by polarized optical microscopy and differential scanning calorimetry (DSC). The optical textures showed typical defects associated with columnar mesophases, and included spiral textures usually observed for columnar oblique mesophases (Col_o), linear birefringent defects and cylindrical domains associated with the columnar rectangular phases (Col_r) and dendritic features, and large areas of uniform extinction found

for columnar hexagonal structures (Col_h). This technique was sufficient to identify the presence of columnar mesomorphism and the existence of columnar hexagonal phases, but did not allow for an unequivocal identification of the lower-symmetry phases, particularly as there are two possibilities for Col_r phases. Consequently, the materials were further studied by X-ray diffraction (vide infra).

The DSC experiments confirmed that the complexes possess excellent thermal stability, clearing to the isotropic liquid in the region 250–300 °C, with very good reproducibility of the mesomorphism on cooling; the reversibility of the thermal behavior was checked with DSC on subsequent heating–cooling cycles. Interestingly, all the complexes crystallized on cooling with no glassy behavior detected. Some general trends are summarized below.

Table 4. Thermodynamic data for all the metal complexes [$MCl_2(L^n)$]. Transition temperatures are given in °C, and the corresponding enthalpies changes are in square brackets [ΔH in kJ mol^{-1}]. Cr: crystalline or solid state; Col_r, Col_o, and Col_h: rectangular, oblique and hexagonal columnar phase, respectively; I: isotropic liquid.

M	*n*	Transitional properties
Zn	8	Cr 111 [28.0] Col_r *c2mm* 138 [–] Col_r *p2gg* 237 [–] Col_r *c2mm* 270 [–] Col_h 285 [10.5] I
	10	Cr 52 [32.9] Col_r *c2mm* 235 [–] Col_h 285 [8.5] I
	12	Cr 48 [55.5] Col_r *c2mm* 170 [–] Col_h 262 [8.0] I
	14	Cr 63 [92.9] Col_r *c2mm* 145 [–] Col_h 248 [5.6] I
	16	Cr 65 [129.0] Col_r *c2mm* 105 [–] Col_h 235 [5.0] I
Co	8	Cr 78 [18.1] Col_o 151 [3.2] Col_r *c2mm* 275 [–] Col_h 303 [8.5] I
	10	Cr 60 [29.9] Col_r *c2mm* 210 [–] Col_h 281 [5.1] I
	12	Cr 46 [33.7] Col_r *c2mm* 175 [–] Col_h 256 [2.8] I
	14	Cr 48 [74.0] Col_r *c2mm* 170 [–] Col_h 258 [4.0] I
	16	Cr 65 [129.0] Col_r *c2mm* 125 [–] Col_h 255 [6.0] I
Mn	8	Cr 83 [30.6] Col_r *c2mm* 185 [–] Col_h 315 [8.8] I
	10	Cr 46 [56.5] Col_r *p2gg* 143 [1.5] Col_h 290 [–] I
	12	Cr 55 [62.4] Col_r *c2mm* 120 [–] Col_h 280 [–] I
	14	Cr 52 [82.3] Col_h 278 [6.8] I
	16	Cr 61 [95.1] Col_h 248 [3.9] I
Ni	8	Cr 148 [94] Col_r *p2gg* 210 [–] Col_r *c2mm* 293 [9.2] I
	10	Cr 90 [11.3] Col_r *c2mm* 125 [–] Col_r *c2mm* 249 [–] Col_h 265 [–] I
	12	Cr 57 [13.8] Col_r *c2mm* 105 [7.7] Col_r *c2mm* 190 [–] Col_h 256 [–] I
	14	Cr 48 [50.8] Col_r *c2mm* 175 [–] Col_h 243 [4.1] I
	16	Cr 62 [71.0] Col_r *c2mm* 155 [–] Col_h 240 [–] I

The clearing temperatures decrease slightly on going from $n=8$ to $n=16$, while the melting points firstly decrease with n, then increase slightly from $n=12$ onwards. The largest mesomorphic temperature range is thus observed for the complexes with $n=10$ and 12. This overall tendency is independent of the metal ion considered. For identical n, the compounds have similar melting points except for the Ni^{II} complexes. These show, on average, the highest values, while a slight discrepancy is observed with the clearing points. Thus, the Mn^{II} and Co^{II} complexes have, on average, a higher clearing point than the analogous Ni^{II} and Zn^{II} compounds. Curiously, however, the mesophase-to-mesophase transitions, with few exceptions only (Table 4), were not observed by DSC probably because they were either too slow or their enthalpies were to low to be detected by the DSC apparatus. Such observations are consistent with those of the dilatometry experiments discussed below.

Characterization by X-ray diffraction (XRD): The different mesophases were further characterized by detailed variable-temperature powder-XRD experiments, with an X-ray pattern being recorded every 20 °C for each compound from the crystalline state up to the isotropic liquid; the transition temperatures detected by DSC and optical microscopy were in good agreement with those derived from XRD. The crystalline phases displayed a series of sharp peaks over the entire range of 2θ. The transformation to the mesophase was accompanied by the disappearance of a number of these sharp reflections and significant changes in intensity in others. The X-ray diffraction patterns supported the results from optical microscopy. This showed that the new complexes exhibited, between them, several columnar mesophases with different 2D symmetries. For mesophases with the same symmetry, qualitatively similar X-ray patterns were obtained whatever the metal center and the chain length, and, broadly, these patterns could be divided up into three different regions.

1) At wide angles, a diffuse and broad-scattering halo was observed centered around 4.5–4.6 Å, corresponding to the liquid-like order (short-range correlations) of the chains bound to the complexes, and thus to the fluid-like nature of the mesophases.
2) At slightly lower angles, another weak, less diffuse halo was seen corresponding to a distance of approximately 5.5–6.5 Å (slightly temperature dependent), which we attribute to the liquid-like correlations between adjacent molecules. This broad scattering suggested a stacking periodicity of the molecular cores inside the columns, although this was not correlated over too great a distance. By analogy with the results of the single-crystal structure determination described above, it is likely that the columns in the mesophase also consist of a time-averaged, alternating arrangement of the molecules. The value of this periodicity will be taken as the repeat unit along the columnar axis, and denoted *h*.
3) Finally, in the small-angle region, a series of sharp Bragg peaks were present, corresponding to both the fundamental and higher orders of reflections, and featuring in all cases columnar mesophases with 2D lattices characteristic of either a Col_h, a Col_r, or a Col_o mesophase. The systematic presence of several reflections indicated the long-range order of the 2D arrangements of the columns, and allowed for an unambiguous phase symmetry assignment.

A detailed indexation of the mesophases of each compound, and the results of these investigations are gathered in Tables 5–8

The various mesophase-to-mesophase transformations could be monitored by the change in the number of peaks, their position, and their relative intensity. Two representative

Table 5. Detailed indexation at a given temperature (T) of all liquid-crystalline phases observed for the Zn complexes.[a]

T [°C]	d_{obs} [Å]	I	hk	d_{calcd} [Å]	Mesophase and parameters
$n=8$: Cr 111 Col_r *c2mm* 138 Col_r *p2gg* 237 Col_r *c2mm* 270 Col_h 285 I					
120	16.9	vs	11	16.9	Col_r *c2mm*
	16.6	vs	20	16.6	$a_r = 33.2$ Å
	9.8	s	31	9.8	$b_r = 19.6$ Å
	9.7	w	02	9.7	$s_r = 652$ Å]^2
	8.5	w	40	8.45	
	8.4	vw	22	8.3	
160	17.3	vs	20	17.3	
	17.0	vs	11	17.0	Col_r *p2gg*
	9.9	s	31	9.9	$a_r = 34.6$ Å
	9.7	w	02	9.75	$b_r = 19.5$ Å
	9.4	w	12	9.4	$s_r = 675$ Å^2
	8.8	m	40	8.65	
	8.5	vw	22	8.45	
240	18.0	vs	20	18.0	Col_r *c2mm*
	17.6	vs	11	17.5	$a_r = 36.0$ Å
	10.3	s	31	10.3	$b_r = 20.2$ Å
	9.0	w	40	9.0	$s_r = 726$ Å^2
280	18.0	vs	10	18.0	Col_h *p6mm*
	10.45	s	11	10.4	$a_h = 20.8$ Å, $S_h = 374$ Å^2
$n=10$: Cr 52 Col_r *c2mm* 235 Col_h 285 I					
120	18.7	vs	20	18.7	Col_r *c2mm*
	18.0	vs	11	18.0	$a_h = 37.4$ Å
	10.3	w	02	10. 3	$s_h = 768$ Å^2
	9.4	w	40	9.35	
	9.0	vw	22	9.0	
240	19.4	vs	10	19.4	Col_h *p6mm*
	11.2	s	11	11.2	$a_h = 22.4$ Å
	9.7	s	20	9.7	$s_h = 435$ Å^2
$n=12$: Cr 48 Col_r *c2mm* 170 Col_h 262 I					
140	20.2	vs	20	20.2	Col_r *c2mm*
	19.75	vs	11	19.75	$a_r = 40.4$ Å
	11.7	s	31	11.6	$b_r = 22.6$ Å
	11.3	w	02	11.3	$s_r = 915$ Å^2
	10.2	w	40	10.1	
	9.9	vw	22	9.9	
180	20.3	vs	10	20.3	Col_h *p6mm*
	11.8	s	11	11.7	$a_h = 23.45$ Å
	11.15	s	20	10.15	$s_h = 476$ Å^2
$n=14$: Cr 63 Col_r *c2mm* 145 Col_h 248 I					
80	21.2	vs	20	21.2	Col_r *c2mm*
	20.3	vs	11	20.1	$a_r = 42.4$ Å
	12.0	s	31	12.05	$b_r = 23.1$ Å
	11.5	w	02	11.6	$s_r = 980$ Å^2
	10.6	w	40	10.6	
	10.0	vw	22	10.15	
240	22.1	vs	10	22.1	Col_h *p6mm*
	12.7	s	11	12.75	$a_h = 25.5$ Å
	11.1	s	20	11.05	$s_h = 564$ Å^2
$n=16$: Cr 65 Col_r *c2mm* 105 Col_h 235 I					
80	22.6	vs	20	22.6	Col_r *c2mm*
	21.6	vs	11	21.6	$a_r = 45.2$ Å
	12.8	s	31	12.8	$b_r = 24.6$ Å
	12.3	s	02	12.3	$s_r = 1111$ Å^2
	11.3	w	40	11.3	
	10.8	vw	22	10.8	
220	23.5	vs	10	23.5	Col_h *p6mm*
	13.6	s	11	13.6	$a_h = 27.1$ Å
	11.8	s	20	11.8	$s_h = 638$ Å^2

[a] d_{obs} and d_{calcd} are the observed and calculated diffraction spacings; I is the intensity of the diffraction signal (vs: very strong, s: strong, m: medium, w: weak, vw: very weak); hk is the indexation of the two-dimensional lattice; a_r, b_r, a_o, b_o, γ, and a_h are the lattice parameters, s_r, s_o, and s_h are the lattice area and *p2gg*, *c2mm*, *p*1, and *p6mm* are the 2D plane groups of the rectangular (Col_r), oblique (Col_o), and hexagonal (Col_h) columnar phases, respectively.

Table 6. Detailed indexation at a given temperature (T) of all liquid-crystalline phases observed for the Co complexes.[a]

T [°C]	d_{obs} [Å]	I	hk	d_{calcd} [Å]	Mesophase and parameters
$n=8$: Cr 78 Col_o 151 Col_r *c2mm* 275 Col_h 303 I					
120	17.8	vs	20	17.8	Col_o *p*1
	16.75	vs	11	16.75	$a_o = 35.7$ Å
	15.9	vs	$1\bar{1}$	15.9	$b_o = 18.4$ Å
	10.2	s	31	10.3	$\gamma = 86.4°$
	9.65	m	$3\bar{1}$	9.7	$s_o = 654.5$ Å^2
	7.55	m	32	7.5	
	7.3	w	51	7.1	
160	17.6	vs	20	17.6	Col_r *c2mm*
	17.0	vs	11	17.0	$a_r = 35.2$ Å
	10.05	s	31	10.05	$b_r = 19.4$ Å
	9.9	w	02	9.7	$s_r = 683$ Å^2
	8.9	w	40	8.8	
	8.6	vw	22	8.5	
280	18.2	vs	10	18.2	Col_h *p6mm*
	10.5	m	11	10.5	$a_h = 21.0$ Å, $s_h = 382.5$ Å^2
$n=10$: Cr 60 Col_r *c2mm* 210 Col_h 281 I					
140	19.1	vs	20	19.1	Col_r *c2mm*
	18.35	vs	11	18.35	$a_r = 38.2$ Å
	10.9	s	31	10.9	$b_r = 20.9$ Å
	10.5	w	02	10.5	$s_r = 799$ Å^2
	9.65	w	40	9.55	
	9.15	vw	22	9.2	
240	19.4	vs	10	19.4	Col_h *p6mm*
	11.2	s	11	11.2	$a_h = 22.4$ Å
	9.7	s	20	9.7	$s_h = 434.5$ Å^2
$n=12$: Cr 46 Col_r *c2mm* 175 Col_h 256 I					
120	20.6	vs	20	20.6	Col_r *c2mm*
	19.75	vs	11	19.75	$a_r = 41.2$ Å
	11.8	s	31	11.7	$b_r = 22.5$ Å
	11.1	w	02	11.25	$s_r = 927$ Å^2
	10.3	w	40	10.3	
	9.8	w	22	9.9	
220	21.1	vs	10	21.1	Col_h *p6mm*
	12.2	s	11	12.2	$a_h = 24.4$ Å
	10.5	s	20	10.5	$s_h = 514$ Å^2
$n=14$: Cr 48 Col_r *c2mm* 170 Col_h 258 I					
80	21.45	vs	20	21.6	Col_r *c2mm*
	20.2	vs	11	20.2	$a_r = 42.9$ Å
	12.1	s	31	12.1	$b_r = 22.9$ Å
	11.45	w	02	11.45	$s_r = 982$ Å^2
	10.8	w	40	10.7	
	10.1	vw	22	10.1	
240	22.45	vs	10	22.45	Col_h *p6mm*
	12.95	s	11	13.0	$a_h = 25.9$ Å
	11.25	s	20	11.2	$s_h = 582$ Å^2
$n=16$: Cr 65 Col_r *c2mm* 125 Col_h 255 I					
120	22.6	vs	20	22.6	Col_r *c2mm*
	22.2	vs	11	22.2	$a_r = 45.2$ Å
	12.9	s	31	13.0	$b_r = 25.5$ Å
	12.75	w	02	12.75	$s_r = 1152$ Å^2
	11.4	w	40	11.3	
	11.1	w	22	11.1	
200	23.3	vs	10	23.3	Col_h *p6mm*
	13.45	s	11	13.45	$a_h = 26.9$ Å
	11.7	s	20	11.65	$s_h = 627$ Å^2

[a] See footnote for Table 5.

X-ray diagrams of the two most commonly encountered columnar phases a) Col_r *c2mm* and b) Col_h) are shown in Figure 5.

The detailed structure of each mesophase will now be described in greater detail.

1) *The columnar hexagonal phases, Col_h*: Below the isotropic liquid, all of the complexes except [$NiCl_2(L^8)$] displayed

Table 7. Detailed indexation at a given temperature (T) of all liquid-crystalline phases observed for the Mn complexes.[a]

T [°C]	d_{obs} [Å]	I	hk	d_{calcd} [Å]	Mesophase and parameters
		$n=8$: Cr 83 Col_r *c2mm* 185 Col_h 315 I			
120	17.1	vs	11	17.1	Col_r *c2mm*
	16.7	vs	20	16.7	$a_r=33.4$ Å
	9.9	s	02	9.9	$b_r=19.9$ Å
	8.7	w	22	8.55	$s_r=665$ Å^2
	8.3	w	40	8.35	
260	18.1	vs	10	18.1	Col_h *p6mm*
	10.45	s	11	10.45	$a_h=20.9$ Å
	9.1	s	20	9.05	$s_h=378$ Å^2
		$n=10$: Cr 46 Col_r *p2gg* 142 Col_h 290 I			
80	18.3	vs	11/20	18.3	Col_r *p2gg*
	10.5	s	31/02	10.6	$a_r=36.6$ Å
	9.05	w	22/40	9.1	$b_r=21.1$ Å
	8.25	w	41	8.4	$a_r/b_r=\sqrt{3}$
	7.7	w	32	8.0	$s_r=773$ Å^2
240	19.5	vs	10	19.5	Col_h *p6mm*
	11.2	s	11	11.25	$a_h=22.5$ Å
	9.7	s	20	9.75	$s_h=439$ Å^2
		$n=12$: Cr 55 Col_r *c2mm* 120 Col_h 280 I			
100	20.1	vs	20	20.1	Col_r *c2mm*
	19.5	vs	11	19.5	$a_r=40.2$ Å
	11.5	s	31	11.5	$b_r=22.3$ Å
	11.15	w	02	11.15	$s_r=896$ Å^2
	10.15	w	40	10.05	
	9.8	vw	22	9.75	
200	20.5	vs	10	20.5	Col_h *p6mm*
	11.8	s	11	11.9	$a_h=23.7$ Å
	10.25	s	20	10.3	$s_h=487$ Å^2
		$n=14$: Cr 52 Col_h 278 I			
140	21.6	vs	10	21.6	Col_h *p6mm*
	12.4	s	11	12.5	$a_h=24.9$ Å
	10.7	s	20	10.8	$s_h=539$ Å^2
240	22.2	vs	10	22.2	Col_h *p6mm*
	12.75	s	11	12.8	$a_h=25.6$ Å, $s_h=569$ Å^2
		$n=16$: Cr 61 Col_h 248 I			
120	22.4	vs	10	22.4	Col_h *p6mm*
	12.9	s	11	12.95	$a_h=25.9$ Å, $s_h=579$ Å^2
	11.2	s	20	11.2	
220	23.5	vs	10	23.5	Col_h *p6mm*
	13.55	s	11	13.6	$a_h=27.1$ Å $s_h=638$ Å^2
	11.65	s	20	11.75	

[a] See footnote for Table 5.

Table 8. Detailed indexation at a given temperature (T) of all liquid-crystalline phases observed for the Ni complexes.[a]

T [°C]	d_{obs} [Å]	I	hk	d_{calcd} [Å]	Mesophase and parameters
		$n=8$: Cr 148 Col_r *p2gg* 210 Col_r *c2mm* 293 I			
160	17.7	vs	11	17.7	Col_r *p2gg*
	15.9	vs	20	15.9	$a_r=31.8$ Å
	10.7	w	02	10.65	$b_r=21.3$ Å
	10.0	s	12	10.1	$s_r=677.5$ Å^2
	9.45	s	31	9.5	
	8.95	s	22	8.85	
	7.45	m	41	7.45	
220	18.35	vs	20	18.35	Col_r *c2mm*
	17.15	vs	11	17.15	$a_r=36.7$ Å, $b_r=19.4$ Å
	10.35	w	31	10.35	$s_r=712$ Å^2
	9.7	s	02	9.7	
		$n=10$: Cr 90 Col_r *c2mm* 125 Col_r *c2mm* 249 Col_h 265 I			
120	19.4	vs	20	19.4	Col_r *c2mm*
	17.75	vs	11	17.75	$a_r=38.8$Å
	10.85	s	31	10.85	$b_r=20.0$ Å
	10.0	w	02	10.0	$s_r=774.5$ Å^2
	8.95	w	22	8.9	
180	19.65	vs	20	19.65	Col_r *c2mm*
	18.45	vs	11	18.45	$a_r=39.3$ Å
	11.1	s	31	11.1	$b_r=20.9$ Å
	10.45	w	02	10.45	$s_r=821$ Å^2
	9.8	w	40	9.8	
	9.2	w	22	9.2	
220	19.25	vs	10	19.25	Col_h *p6mm*
	11.1	s	11	11.1	$a_h=22.2$ Å
	9.7	s	20	9.6	$s_h=429$ Å^2
		$n=12$: Cr 57 Col_r *c2mm* 105 Col_r *c2mm* 190 Col_h 256 I			
60	21.55	vs	20	21.55	Col_{r1} *c2mm*
	18.05	vs	11	18.05	$a_r=43.1$ Å
	11.6	s	31	11.6	$b_r=19.9$ Å
	10.75	w	40	10.7	$s_r=857$ Å^2
	9.9	w	02	9.9	
160	20.9	vs	20	20.9	Col_{r2} *c2mm*
	19.5	vs	11	19.5	$a_r=41.8$ Å
	11.8	s	31	11.8	$b_r=22.0$ Å
	11.2	w	02	11.0	$s_r=921.5$ Å^2
	10.4	w	40	10.4	
200	20.6	vs	10	20.6	Col_h *p6mm*
	11.9	s	11	19.5	$a_h=23.8$ Å
	0.3	s	20	10.3	$s_h=490$ Å^2
		$n=14$: Cr 48 Col_r *c2mm* 175 Col_h 243 I			
80	22.6	vs	20	22.6	Col_r *c2mm*
	20.55	vs	11	20.55	$a_r=45.2$ Å
	12.45	s	31	12.6	$b_r=23.0$ Å
	11.25	w	40	11.3	$s_r=1043$ Å^2
	10.1	w	02	10.3	
220	22.25	vs	11	22.25	Col_h *p6mm*
	12.8	s	11	12.85	$a_h=25.6$ Å
	11.1	s	20	11.1	$S_h=570$ Å^2
		$n=16$: Cr 62 Col_r *c2mm* 155 Col_h 240 I			
120	23.45	vs	20	23.45	Col_r *c2mm*
	22.2	vs	11	22.2	$a_r=46.9$ Å
	13.2	s	31	13.3	$b_r=23.9$ Å
	12.5	w	02	12.6	$s_r=1182$ Å^2
	11.0	w	22	11.1	
160	23.0	vs	10	23.0	Col_h *p6mm*
	13.3	s	11	13.3	$a_h=26.55$ Å
	11.5	s	20	11.5	$s_h=611$ Å^2

[a] See footnote for Table 5.

the hexagonal columnar structure which was confirmed unambiguously by XRD. Thus, three, or occasionally only two, sharp small-angle reflections were observed, with the $1:\sqrt{3}:\sqrt{4}$ reciprocal spacings ratio characteristic of a 2D hexagonal lattice and corresponding to the indexation $(hk)=(10)$, (11) and (20) (Figure 5b). The 2D lattice of the Col_h phase is represented schematically in Figure 6. The columns are located at the nodes of the hexagonal cell (one column per cell), and the columnar axes are perpendicular to this lattice plane. The projection of the cylindrical hard columnar cores onto this lattice plane leads to circular areas separated from one other by the aliphatic medium.[22] The 3D elementary cell is hexagonal.

2) *The columnar rectangular phase, Col_r*: The mesophase appearing below the hexagonal columnar phase was found to possess a 2D rectangular lattice as indicated by the presence in the XRD pattern of the two sharp fundamental peaks. The less intense of these corresponds to the fundamental reflection (20), while the more intense peak is associated with the two reflections (11 and $1\bar{1}$) of equal intensity. For most of the samples, harmonics and higher

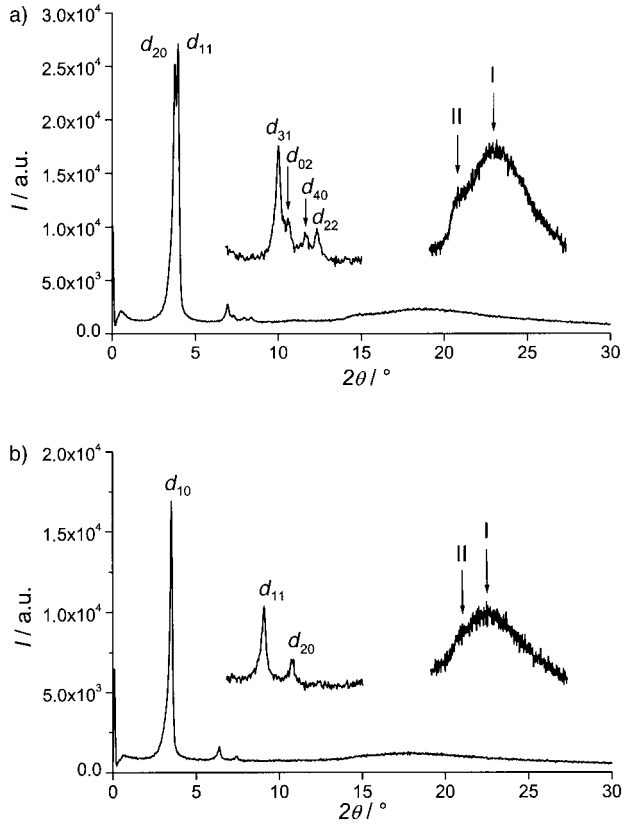

Figure 5. X-ray diffraction patterns of a) $[ZnCl_2(L^{14})]$ at 80°C in Col_r *c2mm*, and b) $[MnCl_2(L^{16})]$ at 180 °C in Col_h *p6mm*.

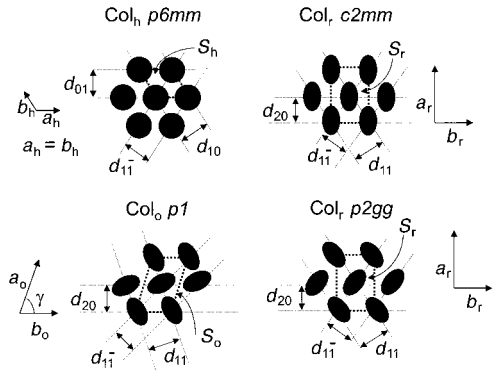

Figure 6. Schematic representation of the 2D lattices of the different columnar mesophases encountered, their associated plane groups, lattice parameters, and surface areas derived from XRD.

orders of diffraction could be observed, allowing the plane group of the Col_r phase to be determined at all temperatures. The rectangular symmetry results from noncylindrical columnar cores, and their projection onto the lattice plane perpendicular to the columnar axis leads to elliptical, time-averaged, columnar cross sections. Such elliptical cross sections are generated either by the molecular shape itself, hindered molecular rotation of non-disklike molecules around the columnar axis, or by the tilt of the molecular disks perpendicular to the columnar axis. Two types of 2D rectangular arrangements of columns are possible for the Col_r mesophases derived from nonchiral mesogens, characterized by two different plane groups, namely *c2mm* and *p2gg*,[22] depending on the mutual orientation of these ellipses in the rectangular lattice (Figure 6). The ellipses are either oriented along a unique direction (*c2mm*) or are alternatively oriented along two different directions (herringbone packing of elliptical columns, *p2gg*). There are now two columns per lattice and the elementary 3D cell is orthorhombic. Both types were observed here, and discrimination between them was made possible due to the number of peaks observed in the X-ray patterns, allowing the reflection conditions for each plane group to be verified (*hk*: $h+k=2n$, *h*0: $h=2n$, 0*k*: $k=2n$ for *c2mm*; *hk*: no conditions, *h*0: $h=2n$, 0*k*: $k=2n$ for *p2gg*). The *p2gg* plane group is less common than its *c2mm* counterpart, the former being assigned for some short chain-length compounds and at lower temperature only. Indeed, the Col_r *p2gg* phase was seen sandwiched between two Col_r *c2mm* for $[ZnCl_2(L^8)]$, between the crystalline phase and the Col_h phase of $[MnCl_2(L^{10})]$, and between the crystalline phase and the Col_r *c2mm* phase of $[NiCl_2(L^8)]$). Interestingly, two compounds ($[ZnCl_2(L^8)]$, $[MnCl_2(L^8)]$) show a Col_r phase just above the crystalline phase with a *c2mm* symmetry, but with the (11) reflection being at the smaller angle, that is, $d_{11} > d_{20}$. The unusual phase sequence between the various Col_r phases observed for the zinc complex could be understood by a transition between a "synclinic" and "anticlinic" Col_r *c2mm* phase, explaining the Col_r *p2gg* one as an intermediate state. The progression of mesomorphic behavior with chain length in the nickel complexes is interesting. For example, in $[NiCl_2(L^8)]$, no enthalpy of transition was detected by DSC between the Col_r *p2gg* and the Col_r *c2mm*; this is not inconsistent with a transition between two phases of the same symmetry, but with different plane groups. However, $[NiCl_2(L^{12})]$ shows a transition from one Col_r (*c2mm*) to another in which the lattice parameters are different and the indices of higher order reflections have been rotated (Table 8). Consistent with a transition between two phases of the same symmetry, they are separated by a first-order phase transition (DSC). However, X-ray evidence suggests that $[NiCl_2(L^{10})]$ also undergoes a transition between two Col_r (*c2mm*) phases, but here the transition is not first-order, or is at least only weakly first-order (DSC). As the presence of higher orders of reflection allows *c2mm* and *p2gg* to be readily identifiable, we are confident of our assignment of the phase symmetries, but cannot account for the absence of a corresponding thermodynamic transition.

3) *The columnar oblique phase, Col_o*: For one compound only ($[CoCl_2(L^8)]$), an oblique *p*1 columnar phase was deduced from the X-ray pattern. Three different fundamental reflections of equal intensity were observed corresponding to the (20), (11) and (1$\bar{1}$) reflections. Note that the 2D lattice does not differ much from a rectangular cell, the angle γ between the lattice parameters a_o and b_o being close to 90° (86.4°). In the Col_o phase, the columnar axis is perpendicular to the normal of the lattice plane (Figure 6), and the projection of the hard cores onto the lattice plane gives rise to a 2D lattice parallelogram which corresponds to the arrangement of the columns, and the elementary cell is monoclinic.[22] Note that here also there are two columns per lattice.

Mesomorphism of the complexes: The results of these detailed X-ray investigations, combined with those from DSC,

allow a complete characterization of the mesomorphic properties, and the thermal behavior of the four series of complexes is summarized in the phase diagrams (Figure 7). One can immediately see, when comparing the four different phase diagrams, that the properties depend on both the chain length and the metal ion. An interesting feature is that for ligands with the same chain length, mesophases of the same symmetry have a different mesophase temperature range and thermodynamic stability which depend on the metal used. For example, the Mn^{II} complexes seem to favor the hexagonal mesophase at the expense of the rectangular one, while this is not consistently true for the Zn^{II}, Co^{II} and Ni^{II} complexes. These differences will be discussed below on the basis of steric factors and microsegregation between the polar hard molecular parts and the nonpolar aliphatic chains. Some classical features of columnar mesomorphism are nevertheless observed. Thus, as n increases, the stability of the hexagonal columnar phase increases at the expense of the temperature range of the rectangular mesophase. Further, the Col_h phase was always seen at higher temperatures than the Col_r, which themselves were seen above the Col_o phase.

Packing study: From a geometrical point of view, the columnar structures are characterized mainly by two parameters: the columnar cross section (S) and the stacking periodicity along the columnar axis (h).[23] Knowledge of these two structural parameters permits interpretation of the molecular packing inside the columns and a better understanding of the influence of this packing on the 2D arrangement of the columns, and, therefore on the mesophase symmetry. In the following, emphasis will be placed on the analysis of the variations of h and S with both n and T. The complexes reported here are amphiphilic, being formed by two distinct parts, which are mutually incompatible (i.e., a polar core surrounded by peripheral aliphatic chains) and well separated in space. Consequently, their liquid-crystalline structures can be described in terms of microphase segregation.[24]

The periodicity (h), the columnar cross section (S), and the molecular volume (V_{mol}) are linked analytically through the now well-established relation given in Equation (1):[23]

$$hS = NV_{mol} \quad (1)$$

in which N is the number of molecules within a volume fraction of column; hS also equals to the volume of the columnar cell, V_{cell}. Note that h is obtained directly from the X-ray patterns (see above), and the molecular volume (V_{mol}) and the cross-sectional area of the columns (Tables 5–8) were also determined experimentally by dilatometry and XRD.

Prior to the analysis of h, the molecular volume was measured experimentally by dilatometry and its variation as a function of temperature followed for one sample ([$ZnCl_2(L^{16})$]. The experiment was carried out, with approximately one gram of compound, between room temperature and 200 °C, and included the C_r-to-Col_r and Col_r-to-Col_h phase transformations (Figure 8). At about 60 °C, the melting of the sample was detected by an abrupt increase in the molecular volume. Then, above this transition, its temperature variation is quasi-linear, despite the change from one mesophase to another.[25] The slope is in fairly good agreement with the volume variation in the methylene groups in liquid alkanes,[26] an indication that the volume of the aromatic part (V_{Ar})[27] is almost unchanged with temperature in the mesophase. In

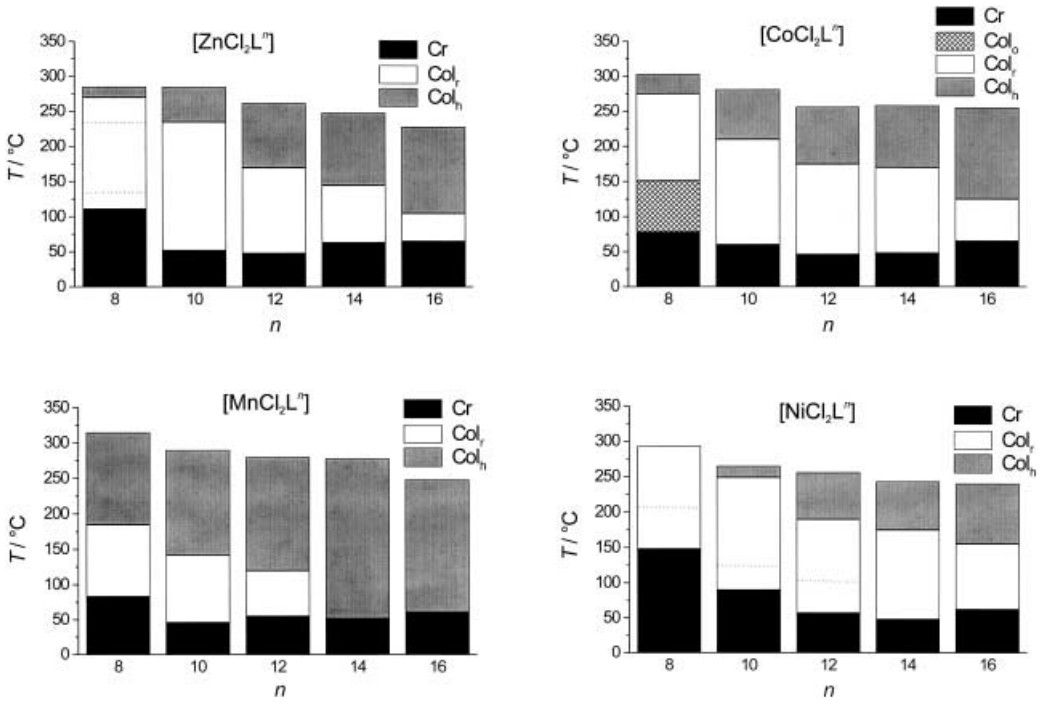

Figure 7. Phase diagrams of the different series of complexes. The dotted lines correspond to transitions between the different Col_r phases within the same compound.

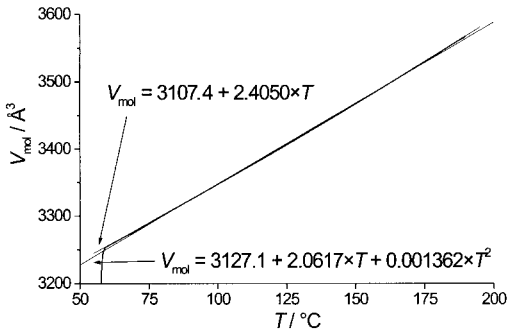

Figure 8. Temperature-dependence of the molecular volume of $[ZnCl_2(L^{16})]$.

fact, only a slight increase in the dilation coefficient could be measured at the Col_r-to-Col_h transition (105 °C).[28] In the following discussion, V_{mol} has been considered to vary linearly over the entire mesomorphic temperature range.

Due to the amphiphilic character of the materials, it is possible to extrapolate the molecular volume of all the other complexes by using the additivity rule of the partial volume, as demonstrated previously.[29] The volume of the central rigid part of the molecule (V_{Ar})[30] was assumed to remain unchanged for the four types of complexes, a reasonable hypothesis taking into account their structural similarity and the chain volume fraction which is the dominant factor. A general analytical expression [Eq. (2)] for the molecular volume[31] as a function of both T and n was thus deduced for all complexes (V_{mol} in Å^3, and T in °C).

$$V_{mol} = 577.2 + 0.12\,T + 0.00136\,T^2 + 6nV_{CH_2} \quad (2)$$

The variation of the columnar cross section (S) was analyzed as a function of both temperature and chain length for all complexes, allowing for the fact that the value of S depends on the symmetry of the mesophases. In the case of the hexagonal mesophase, the cross section S of the columns corresponds exactly to the lattice area, s_h (Figure 6), and is directly calculated from the measurement of d_{10}.[32] For the rectangular and oblique columnar phases, the unit cell of s_r and s_o each contains two columns (Figure 6)[20] defined by the three fundamental reflections (d_{20}, d_{11}, $d_{1\bar{1}}$) and the angle γ. The mathematical expression for these lattice areas is given in a footnote.[33] Thus, $S = s_r/2 = s_o/2$ for the columnar cross sections of the rectangular and oblique phases (the linear analytical expressions for S are added as Supporting Information). As can be seen from the curves (Figure 9), the columnar areas increase linearly with T for all M with no discontinuity, despite the presence of several mesophase transformations (see Table 4). Similarly, and as expected, S increases linearly with increasing chain length but at a higher rate for higher values of n. These variations of S imply that only small structural changes take place at the molecular level and that the integrity of the columnar core is preserved during the phase transformations.

Tilting of the molecular planes with respect to the columnar axis, chain conformations and/or core–core lateral translations are usually responsible for the distortion of 2D lattices, and thus for the mesophase transformations, while higher energy changes such as intercolumnar molecular fluctuations are not. This assumption is supported by the absence in the DSC traces of measurable enthalpies at most phase transformations, an indication that most of these transitions occur with small changes only. The composition of the repeat unit

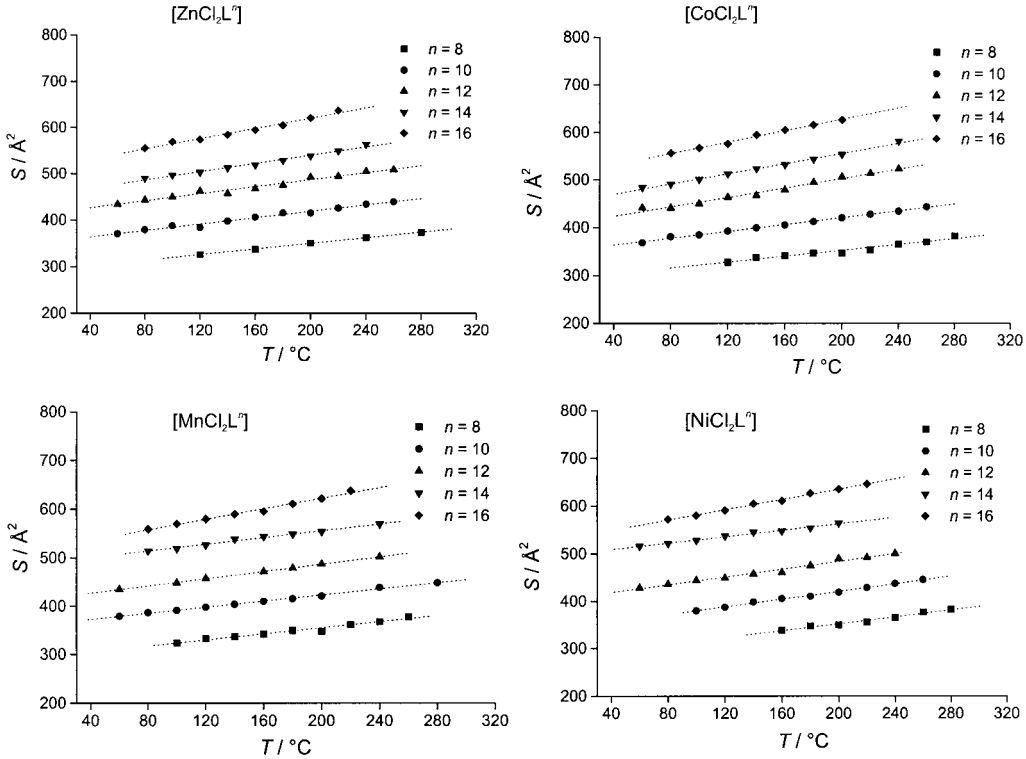

Figure 9. Variation of the columnar cross-section areas (S) with T for each member of the Zn^{II}, Co^{II}, Mn^{II}, and Ni^{II} series.

(i.e., the number of molecules per elementary cell) for the columnar phases Col_r, Col_o, and Col_h should remain effectively constant. Moreover, for almost all the Col_r mesophases and the Col_o mesophase, the observed increase in S correlates with the increase in the lattice parameter a, while the b parameter remains almost constant. In particular, for the Col_r phase with $c2mm$ symmetry, the ratio of the lattice parameters (a_r/b_r) increases and diverges quite substantially from $\sqrt{3}$ upon increasing temperature or n. First accepting that our core is considered as a back-to-back "dimer" of two complexes, we can understand this on the molecular level as follows. Thus, in the Col_r phase, the core is tilted (elliptical cross sections are required to generate phases of rectangular symmetry), but as we increase the temperature, the chains increase their effective volume through thermally induced motion. This increase in volume requires the core to tilt towards an orientation perpendicular to the columnar axis, thus increasing the observed cross section, S. The change in tilt can be considered as resulting exclusively from the rotation of the ab plane around the b axis and, hence, the a parameter increases, while b remains unaffected. As the temperature increases further, the tilt of the core reduces further, S continues to increase, and, eventually, the "dimer" presents a circular cross section to the columnar axis and the transition to the hexagonal phase is complete.

The average thickness of the repeat unit can now be evaluated as a function of T, n, and the metal by combining the analytical expressions of S and V_{mol} in Equation (3). Based on the crystalline structure and on the molecular shape, it is reasonable to consider that only one molecule (half a dimer) is contained within the columnar cell of thickness h, and the parameters measured are comparable to the molecular dimensions. Therefore, $N = 1$ in Equation 1.

$$h = V_{mol}/S \tag{3}$$

The results of these calculations are plotted in Figure 10. The repeat period (h) is close to invariant with temperature or shows a small decrease which is nonlinear, that is, h decreases almost linearly in the lower temperature range and then reaches a plateau with a fixed value at higher T, at which most of the samples are in the Col_h phase. The variation in h is almost the same for the four series of complexes, and its average value ($\langle h \rangle$) is approximately centered around 6 Å ($h_{max} \approx 6.5$ Å; $h_{min} \approx 5.5$ Å). Note that for two compounds ([$MnCl_2(L^{14})$] and [$NiCl_2(L^{14})$]), h was found to be almost independent of temperature. Nevertheless, on average, this measured distance matches the d spacing of the second broad halo measured by XRD (vide supra) in the mesophases, and, therefore, supports its assignment as being the columnar repeat parameter. Furthermore, in the crystalline state, a similar distance was found for the Ni···Ni separations: 6.5 Å and 6.8 Å. Thus, this overall decrease in h corresponds to a slight approach of two neighboring molecules in the direction of the columnar axis. This approach can be understood by the above postulation of a decrease in the tilt angle of the molecular cores, driven by the effective increase in the volume of the aliphatic chains. Once the chains are fully expanded around the columnar core, h becomes invariant.

The variation in S_{Ar}, the cross section of the columnar core, has also been analyzed, and gives a confirmation of the above explanations. Values of S_{Ar} can be readly calculated, since the volume fraction of the columnar core, X_{Ar}, can be defined by Equation (4).

$$S_{Ar} = S(V_{Ar}/V_{mol}) = X_{Ar}S \tag{4}$$

S_{Ar} varies as a quadratic function of T and increases slightly for the four series of metallomesogens. Within each series and for all n, S_{Ar} converges towards 70–75 Å^2 in the high-

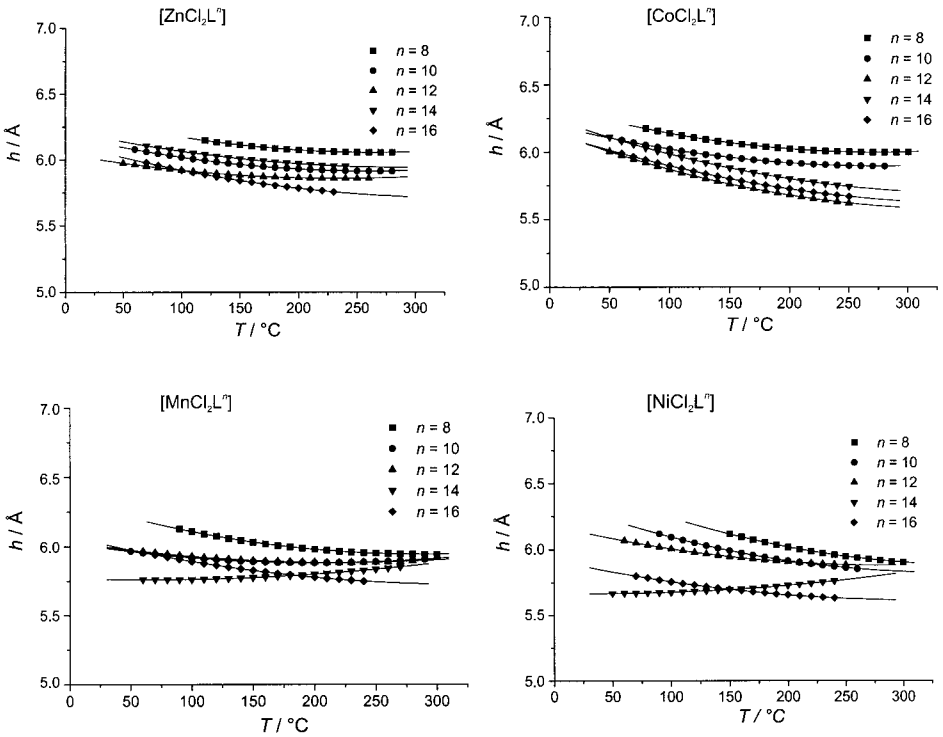

Figure 10. Variation of h with T for each member of the Zn^{II}, Co^{II}, Mn^{II}, and Ni^{II} series.

temperature Col_h phase (Figure 11). The variation of S_{Ar} seems to depend on the metallic center. In the higher temperature part of the diagram, S_{Ar} increases at a slower rate than in the lower temperature range. The temperature behavior of S_{Ar} is associated with a decreasing tilt angle of the molecular plane, in good agreement with the variation in *h*. Once again, the influence of the increase in chain volume is crucial.

To summarize, the variation in several parameters has been followed as a function of *n*, *T*, and the metal, allowing for a model of the molecular organization within the columns to be proposed and to investigate how these factors drive mesophase–mesophase transitions. The parameters *S*, S_{Ar}, and V_{mol} increase with both *T* and *n*, as expected, while *h* decreases with no clear dependence on *n* being evident. Owing to their coordination geometry mode, the complexes also exhibit a lateral dipole moment. While such an energetically favorable dipole–dipole interaction between molecules will be favored by the stacking of the molecules in an antiparallel disposition, the driving force is due to the steric effects and spatial requirements of the aliphatic chains, since the antiparallel distribution of the alkoxy chains along the columns gives rise to a more efficient space-filling. Thus, in this way, each pair of molecules completes a disklike shell of chains surrounding the rigid part of the complex (Figure 12).

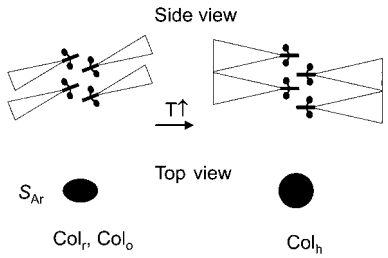

Figure 12. Schematic illustration of the packing modes of the complexes in the columnar phases.

Conclusions

A new liquid-crystalline metallomesogen system based on Zn^{II}, Co^{II}, Mn^{II}, and Ni^{II} centers complexed to 2,6-bis[3′,4′,5′-tri(alkoxy)phenyliminomethyl]pyridine ligands has been developed. The complexes were prepared by a template synthesis and obtained in good yields; their characterization indicated the formation of 1:1 metal–ligand products. Crystal structure determinations of $[NiCl_2(L^1)]$, $[ZnCl_2(L^1)]$, and $[MnCl_2(L^1)]$ confirmed that the metal is bound by the terdentate Schiff base ligand (L) and by two chloride ions to give an distorted trigonal bipyramidal coordination geometry. All the 1:1 complexes exhibit columnar mesophases that are stable at high temperatures, and exist over broad temperature ranges. Increasing the chain length or changing the metal does not affect the thermal stability of the complexes, but does influence strongly the nature of the two-dimensional packing of the columns in the cells. The mesomorphism is explained on the basis of the steric demands of the aliphatic chains, which confine the rigid part together, promoting the favorable, antiparallel arrangement of the molecular dipoles. Such an arrangement of these half-disk compounds produces a columnar structure composed of repeat units of either circular or elliptical cross section.

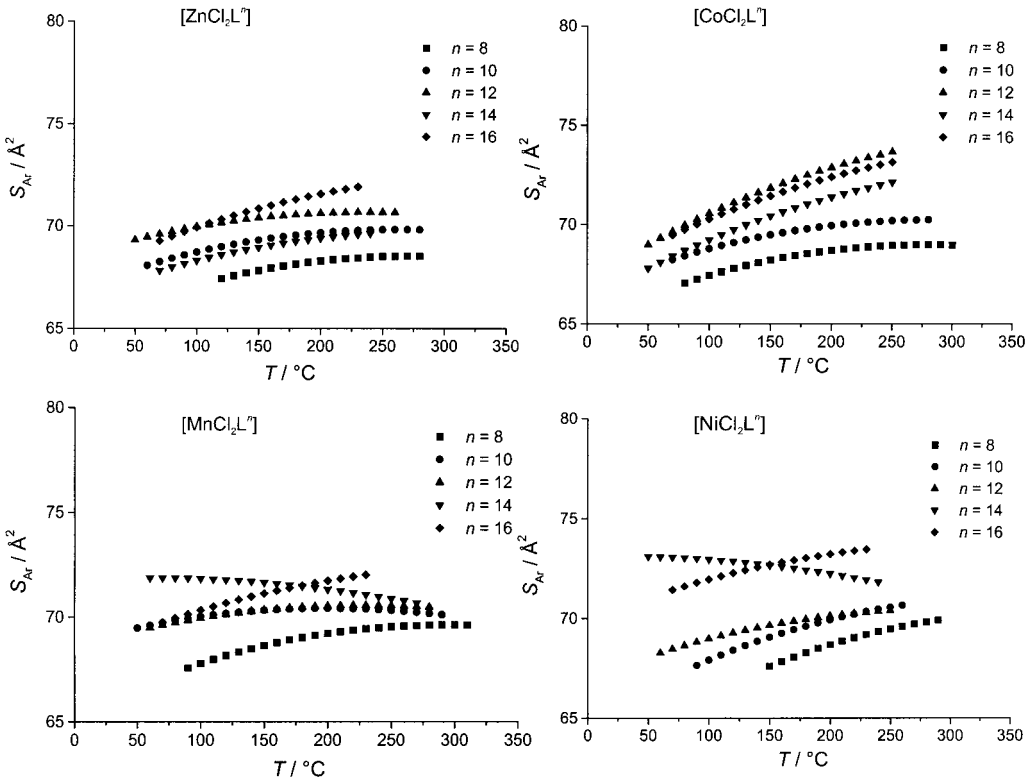

Figure 11. Variation of S_{Ar} (area of the rigid part of the columns) with *T* for each member of the Zn^{II}, Co^{II}, Mn^{II}, and Ni^{II} series.

Experimental section

Materials: All chemicals were purchased from commercial suppliers and were used without further purification. The EtOH used in the preparation of the anilines was dried over Mg turnings and freshly distilled prior to use. The series of 3,4,5-tri(alkoxy)anilines were prepared according to a published method.[19]

Instrumentation: NMR spectra were recorded on a Bruker DPX300 FT-NMR spectrometer operating at 300.13 MHz for ^{1}H and 75.48 MHz for ^{13}C. Chemical shifts are referenced with respect to residual proton or carbon solvent. IR spectra were recorded as KBr pellets on a Nicolet AVATAR 360 FTIR spectrometer. UV/Vis spectra were measured on a Philips PU 8720 spectrophotometer. FAB mass spectra were obtained on a Finnigan MAT TSQ-700 at the University of Wales, Swansea, with 3-nitrobenzyl alcohol (NOBA) as matrix. Elemental analyses (C, H, N) were carried out by the Analytical Department of the University of Nottingham. Measurements of conductivity were made using a Jenway 4010 conductivity meter with $CHCl_3$ as solvent.

The transition temperatures and enthalpy changes were measured by differential scanning calorimetry using a Perkin–Elmer DSC-7 instrument operated at a scanning rate of 10 °C min^{-1} on heating. The apparatus was calibrated with indium (156.6 °C; 28.4 J g^{-1}) as the standard.

Dilatometry measurements were performed by using a high precision locally constructed apparatus, with automatic computer control of data-acquisition and temperature (within ±0.03 °C).

The XRD patterns were obtained with two different experimental set-ups. In the first set, a linear monochromatic $Cu_{K\alpha 1}$ beam ($\lambda = 1.5405$ Å) was obtained by using a Guinier camera with a sealed-tube generator (900 W). In the second, a Debye–Scherrer camera equipped with a bent quartz monochromator and an electric oven was used. In both cases, the crude powder was filled in Lindemann capillaries of 1 mm diameter. An initial set of diffraction patterns was recorded with a curved Inel CPS 120 gas-filled detector linked to a data acquisition computer; periodicities up to 60 Å could be measured, and the sample temperature controlled to within ±0.05 °C. The second set of diffraction patterns was recorded on an image plate; cell parameters of the Col_r and Col_o mesophases were calculated from the position of the reflection at the smallest Bragg angle, which was in all cases the most intense; the hexagonal cell parameter was calculated by using all the reflections $a = (2/3\sqrt{3})(d_{10} + \sqrt{3}d_{11} + 2d_{20})$. Periodicities up to 90 Å could be measured, and the sample temperature controlled to within ±0.3 °C. In each case, exposure times were varied from 1 to 24 h depending on the mesophase observed and upon the specific reflections being sought (weaker reflections obviously taking longer exposure times).

X-ray crystallographic data collection and refinement of the structures: All single-crystal diffraction data were collected on a Bruker SMART1000 CCD area detector diffractometer,[34] equipped with an Oxford Cryosystems open-flow nitrogen cryostat,[35] with graphite-monochromated $Mo_{K\alpha}$ radiation ($\lambda = 0.71073$ Å). Crystal data for the compounds $[MnCl_2(L^1)]\cdot 0.5\,PhCN$, $[NiCl_2(L^1)]\cdot PhCN$, $[NiCl_2(L^1)]\cdot PhNO_2$, and $[ZnCl_2(L^1)]\cdot 0.5\,PhCN$ are listed in Table 1. Integrated intensities, corrected for Lorentz and polarization effects, were obtained using the Bruker SAINT package,[36] as were the cell parameters. All data were corrected for absorption by using a multi-scan method.[37] $[NiCl_2(L^1)]\cdot PhCN$ was solved by using heavy-atom methods; $[MnCl_2(L^1)]\cdot 0.5\,PhCN$, $[NiCl_2(L^1)]\cdot PhNO_2$ and $[ZnCl_2(L^1)]\cdot 0.5\,PhCN$ were solved by using direct methods[38] and all further non-hydrogen atoms were located in subsequent difference Fourier syntheses. Full-matrix least-squares refinement on F^2 was carried out by using SHELXL-97.[39] All hydrogen atoms were placed in geometrically calculated positions and refined as riding on the parent atoms. Distance restraints were applied to the phenyl ring of the benzonitrile molecule in $[NiCl_2(L^1)]\cdot PhCN$. The benzonitrile solvent molecules in $[MnCl_2(L^1)]\cdot 0.5\,PhCN$ and $[ZnCl_2(L^1)]\cdot 0.5\,PhCN$ were disordered over inversion centers; they were modeled over two half-occupied sites and sensible geometric restraints applied. All the partially occupied atoms described above were refined with isotropic displacement parameters, and other non-hydrogen atoms with anisotropic displacement parameters. All hydrogen atoms were placed in geometrically calculated positions and refined riding on parent atoms.

Synthesis of 2,6-bis[3′,4′,5′-tri(methoxy)phenyliminomethyl]pyridine (L^1): A mixture of 2,6-pyridinedicarboxaldehyde (0.152 g, 1.12 mmol) and 3,4,5-trimethoxyaniline (0.412 g, 2.25 mmol) was heated under reflux in MeOH (150 mL) for 4 h; this resulted in a yellow solution that was left to evaporate at room temperature. The precipitate that formed after 24 h was collected by filtration and washed with a small amount of cold MeOH, affording a yellow crystalline solid in 62% yield (0.325 g). ^{1}H NMR (300.13 MHz, $CDCl_3$): $\delta = 8.71$ (s, 2H; HC=N), 8.27 (d, $^3J(H,H) = 7.4$ Hz, 2H; Py–$H_{3/5}$), 7.94 (t, $^3J(H,H) = 7.4$ Hz, 1H; Py–H_4), 6.63 (s, 4H; Ar–H), 3.90 (s, 12H; m-OCH_3), 3.88 (s, 6H; p-OCH_3); ^{13}C NMR (75.48 MHz, $CDCl_3$): $\delta = 158.99$ (HC=N), 154.67 (Py–C_4), 153.74 (C_q), 146.38 (C_q), 137.49 (C_q), 123.31 (Py–$C_{3/5}$), 98.83 (Ar–C_2), 61.08 (p-OCH_3), 56.23 ppm (m-OCH_3); IR (KBr): $\tilde{\nu} = 1587$ cm^{-1} (C=N); FAB-MS: m/z: 466 $[M]^+$; UV/Vis ($CHCl_3$): λ_{max} (ε) = 243 (3.2×10^4), 354 nm (2.5×10^4 mol^{-1} dm^3 cm^{-1}); elemental analysis calcd (%) for $C_{25}H_{27}N_3O_6$: C 64.50, H 5.85, N 9.03; found: C 64.23, H 5.76, N 8.98.

Synthesis of 2,6-bis[3′,4′,5′-tri(hexadecyloxy)phenyliminomethyl]pyridine (L^{16}): The same proceedure was used for the preparation of L^{16}, but with pyridinedicarboxaldehyde (0.0428 g, 0.317 mmol) and 3,4,5-tri(hexadecyloxy)aniline (0.516 g, 0.634 mmol). Appearance: yellow solid in 65% yield (0.356 g); ^{1}H NMR (300.13 MHz, $CDCl_3$): $\delta = 8.69$ (s, 2H; HC=N), 8.23 (d, $^3J(H,H) = 7.8$ Hz, 2H; Py-$H_{3/5}$), 7.92 (t, $^3J(H,H) = 7.8$ Hz, 1H; Py-H_4), 6.61 (s, 4H; Ar-H), 4.03–3.96 (m, 12H; OCH_2), 1.85–1.26 (m, 168H; CH_2), 0.88 ppm (2 overlapping triplets, 18H; CH_3); ^{13}C NMR (75.48 MHz, $CDCl_3$): $\delta = 158.46$ (HC=N), 154.74 (Py-C_4), 153.52 (C_q), 145.76 (C_q), 137.46 (C_q), 123.00 (Py-$C_{3/5}$), 100.13 (Ar-C_2), 73.59 (OCH_2), 69.17 (OCH_2), 31.94, 30.38, 29.73, 29.39, 26.13, 22.70 (CH_2), 14.11 ppm (CH_3); IR (KBr): $\tilde{\nu} = 1585$ cm^{-1} (C=N); FAB-MS: m/z: 1726 $[M]^+$; UV/Vis ($CHCl_3$): λ_{max} (ε) = 241 (3.1×10^4), 360 nm (2.4×10^4 mol^{-1} dm^3 cm^{-1}); elemental analysis calcd (%) for $C_{115}H_{207}N_3O_6$: C 79.94, H 9.50, N 2.43; found: C 80.42, H 9.45, N 2.36.

Genaral preparation of the 2,6-bis[3′,4′,5′-tri(alkoxy)phenyliminomethyl]-pyridinedichlorometal(II) complexes: A solution of 2,6-pyridinedicarboxaldehyde (0.0133 g, 0.0984 mmol) and 3,4,5-trimethoxyaniline (0.0361 g, 0.197 mmol) in $CHCl_3$ (20 mL) was stirred at room temperature for 10 min, before adding a solution of $NiCl_2\cdot 6H_2O$ (0.0234 g, 0.0984 mmol) in EtOH (7.5 mL). The deep-red solution was heated under reflux for 20 h and then left to evaporate at room temperature until a crystalline brick-red solid precipitated. The product was collected by filtration and washed with a small amount of cold EtOH, with a yield of 0.0498 g (85%). IR (KBr): $\tilde{\nu} =$ 1590 cm^{-1} (C=N); FAB-MS: m/z: 524 $[M-2Cl]^+$, 559 $[M-Cl]^+$; UV/Vis (CHCN): λ_{max} (ε) = 208 (9.0×10^4), 281 (1.9×10^4), 387 nm (2.1×10^4 mol^{-1} dm^3 cm^{-1}); elemental analysis calcd (%) for $C_{25}Cl_2H_{27}N_3O_6Ni$: C 50.46, H 4.57, N 7.06; found: C 50.13, H 4.49, N 7.11. X-ray quality crystals of the product were grown by the layering of 2,6-bis-[3,4,5-tri(methoxy)phenylimine]pyridine (0.0120 g, 0.0258 mmol) in benzonitrile (1.5 mL) and $NiCl_2\cdot 6H_2O$ (0.0061 g, 0.0257 mmol) in EtOH (1.5 mL) over 4 weeks, into which n-pentane was subsequently diffused to form orange tablets. Another batch of orange tablet-like crystals was obtained by diffusion of n-pentane into nitrobenzene solution. The same synthetic procedure was used for the preparation of the other nickel complexes.

[NiCl$_2$(L^8)]: This complex was prepared from pyridinedicarboxaldehyde (0.0190 g, 0.141 mmol), 3,4,5-tri(octyloxy)aniline (0.134 g, 0.280 mmol), $NiCl_2\cdot 6H_2O$ (0.0334 g, 0.141 mmol) in EtOH (9 mL). The precipitate, formed by reducing the solvent volume, was collected by filtration and washed with a small amount of cold EtOH. Appearance: orange-red solid (56%, 0.0932 g); IR (KBr): $\tilde{\nu} = 1589$ cm^{-1} (C=N); FAB-MS: m/z: 1112 $[M-2Cl]^+$, 1147 $[M-Cl]^+$; UV/Vis ($CHCl_3$): λ_{max} (ε) = 244 (2.8×10^4), 288 (1.0×10^4), 388 (1.7×10^4), 429 nm (1.7×10^4 mol^{-1} dm^3 cm^{-1}). The microanalysis gives satisfactory results with one molecule of water. Elemental analysis calcd (%) for $C_{67}Cl_2H_{111}N_3O_6Ni\cdot 1H_2O$: C 66.94, H 9.47, N 3.50; found: C 66.53, H 9.49, N 3.25.

[NiCl$_2$(L^{10})]: This complex was prepared from pyridinedicarboxaldehyde (0.022 g, 0.163 mmol), 3,4,5-tri(decyloxy)aniline (0.183 g, 0.326 mmol), and $NiCl_2\cdot 6H_2O$ (0.0387 g, 0.163 mmol). Appearance: orange-red solid (0.1760g, 78%); IR (KBr): $\tilde{\nu} = 1590$ cm^{-1} (C=N); FAB-MS: m/z: 1280 $[M-2Cl]^+$; UV/Vis ($CHCl_3$): λ_{max} (ε) = 242 (2.0×10^4), 290 (9.0×10^3), 389 (1.2×10^4), 427 nm (1.1×10^4 mol^{-1} dm^3 cm^{-1}). The microanalysis gives satisfactory results with two molecules of water. Elemental analysis calcd (%) for $C_{79}Cl_2H_{135}N_3O_6Ni\cdot 2H_2O$: C 68.34, H 10.09, N 3.03; found: C 68.60, H 10.01, N 3.00.

[$NiCl_2(L^{12})$]: This complex was prepared from pyridinedicarboxaldehyde (0.013 g, 0.158 mmol), 3,4,5-tri(dodecyloxy)aniline (0.204 g, 0.316 mmol), and $NiCl_2 \cdot 6H_2O$ (0.0375 g, 0.158 mmol). Appearance: crystalline orange solid (0.151 g, 63%); IR (KBr): $\tilde{\nu} = 1589\ cm^{-1}$ (C=N); FAB-MS: *m/z*: 1448 $[M-2Cl]^+$, 1483 $[M-Cl]^+$; UV/Vis ($CHCl_3$): λ_{max}, (ε) = 246 (1.6×10^4), 288 (5.9×10^3), 394 (9.8×10^3), 432 nm ($9.7 \times 10^3\ mol^{-1}\,dm^3\,cm^{-1}$); elemental analysis calcd (%) for $C_{91}Cl_2H_{159}N_3O_6Ni$: C 71.87, H 10.54, N 2.76; found: C 71.38, H 10.66, N 2.71.

[$NiCl_2(L^{14})$]: This complex was prepared from pyridinedicarboxaldehyde (0.0198 g, 0.147 mmol), 3,4,5-tri(tetradecyloxy)aniline (0.214 g, 0.293 mmol), and $NiCl_2 \cdot 6H_2O$ (0.0348 g, 0.146 mmol); appearance: yellow-orange solid (0.172 g, 67%); IR (KBr): $\tilde{\nu} = 1589\ cm^{-1}$ (C=N); FAB-MS: *m/z*: 1617 $[M-2Cl]^+$, 1653 $[M-Cl]^+$; UV/Vis ($CHCl_3$): λ_{max} (ε) = 246 (2.4×10^4), 288 (8.9×10^3), 383 (1.3×10^4), 440 nm ($1.3 \times 10^4\ mol^{-1}\,dm^3\,cm^{-1}$). The microanalysis gives satisfactory results with three molecules of water. Elemental analysis calcd (%) for $C_{103}Cl_2H_{183}N_3O_6Ni \cdot 3H_2O$: C 70.97, H 10.93, N 2.41; found: C 70.49, H 10.98, N 2.56.

[$NiCl_2(L^{16})$]: This complex was prepared from pyridinedicarboxaldehyde (0.0204 g, 0.151 mmol), 3,4,5-tri(hexadecyloxy)aniline (0.246 g, 0.302 mmol), and $NiCl_2 \cdot 6H_2O$ (0.0359 g, 0.151 mmol). Appearance: crystalline orange solid (0.239 g, 80%); IR (KBr): $\tilde{\nu} = 1586\ cm^{-1}$ (C=N); FAB-MS: *m/z*: 1784 $[M-2Cl]^+$; UV/Vis ($CHCl_3$): λ_{max} (ε) = 252 (2.6×10^4), 290 (9.5×10^3), 343 (1.7×10^4), 435 nm ($1.7 \times 10^4\ mol^{-1}\,dm^3\,cm^{-1}$). The microanalysis gives satisfactory results with one molecule of chloroform. Elemental analysis calcd (%) for $C_{115}Cl_2H_{207}N_3O_6Ni \cdot CHCl_3$: C 70.48, H 10.61, N 2.13; found: C 70.24, H 11.00, N 2.06; conductivity ($CHCl_3$): $\Lambda = 0\ S\,m^{-2}\,mol^{-1}$.

[$MnCl_2(L^1)$]: A solution of 2,6-pyridinedicarboxaldehyde (0.0160 g, 0.118 mmol) and 3,4,5-tri(methoxy)aniline (0.0434 g, 0.237 mmol) in $CHCl_3$ (20 mL) was stirred at room temperature for 10 min. The subsequent addition of a solution of $MnCl_2 \cdot 4H_2O$ (0.0234 g, 0.118 mmol) in EtOH (7.5 mL) caused an orange solid to form in suspension, and stirring of the mixture was carried out for a further 24 h. The fine crystalline light orange precipitate was isolated by filtration in 93% yield (0.0651 g). IR (KBr): $\tilde{\nu} = 1588\ cm^{-1}$ (C=N); FAB-MS: *m/z*: 521 $[M-2Cl]^+$, 556 $[M-Cl]^+$. The microanalysis gives satisfactory results with three molecules of water. Elemental analysis calcd (%) for $C_{25}Cl_2H_{27}N_3O_6Mn \cdot 3H_2O$: C 46.53, H 5.15, N 6.51; found: C 46.44, H 4.08, N 6.64.

[$MnCl_2(L^8)$]: A solution of 2,6-pyridinedicarboxaldehyde (0.0130 g, 0.0962 mmol) and of 3,4,5-tri(octyloxy)aniline (0.0919 g, 0.192 mmol) in $CHCl_3$ (20 mL) was stirred at room temperature for 10 min, before a solution of $MnCl_2 \cdot 4H_2O$ (0.0190 g, 0.0960 mmol) in EtOH (7.5 mL) was added. The golden-brown reaction mixture was stirred at room temperature for 20 h and then left to evaporate for 2 days. The resulting precipitate was filtered off and washed with a small amount of cold EtOH, affording light-brown needles in 75% yield (0.0855 g). IR (KBr): $\tilde{\nu} = 1589\ cm^{-1}$ (C=N); FAB-MS: *m/z*: 1144 $[M-Cl]^+$; UV/Vis ($CHCl_3$): λ_{max} (ε) = 247 (2.5×10^4), 293 (8.7×10^3), 441 nm ($1.8 \times 10^4\ mol^{-1}\,dm^3\,cm^{-1}$); elemental analysis calcd (%) for $C_{67}Cl_2H_{111}N_3O_6Mn$: C 68.17, H 9.48, N 3.56; found: C 68.27, H 9.64, N 3.75.

[$MnCl_2(L^{10})$]: This complex was prepared from pyridinedicarboxaldehyde (0.0152 g, 0.112 mmol), 3,4,5-tri(decyloxy)aniline (0.126 g, 0.224 mmol), and $MnCl_2 \cdot 4H_2O$ (0.0223 g, 0.113 mmol). Appearance: crystalline red-brown solid (0.124 g, 82%); IR (KBr): $\tilde{\nu} = 1584\ cm^{-1}$ (C=N); FAB-MS: *m/z*: 1312 $[M-Cl]^+$; UV/Vis ($CHCl_3$): λ_{max} (ε) = 247 (2.6×10^4), 295 (8.4×10^3), 441 nm ($1.9 \times 10^4\ mol^{-1}\,dm^3\,cm^{-1}$); elemental analysis calcd (%) for $C_{79}Cl_2H_{135}N_3O_6Mn$: C 70.35, H 10.09, N 3.12; found: C 70.83, H 10.39, N 3.30.

[$MnCl_2(L^{12})$]: This complex was prepared from pyridinedicarboxaldehyde (0.0147 g, 0.109 mmol), 3,4,5-tri(dodecyloxy)aniline (0.141 g, 0.218 mmol), and $MnCl_2 \cdot 4H_2O$ (0.0215 g, 0.109 mmol). Appearance: brown solid (0.086 g, 52%); IR (KBr): $\tilde{\nu} = 1585\ cm^{-1}$ (C=N); FAB-MS: *m/z*: 1480 $[M-Cl]^+$; UV/Vis ($CHCl_3$): λ_{max} (ε) = 244 (2.4×10^4), 292 (8.6×10^3), 440 nm ($1.8 \times 10^4\ mol^{-1}\,dm^3\,cm^{-1}$); elemental analysis calcd (%) for $C_{91}Cl_2H_{159}N_3O_6Mn$: C 72.05, H 10.56, N 2.77; found: C 71.98, H 10.62, N 2.57.

[$MnCl_2(L^{14})$]: This complex was prepared from pyridinedicarboxaldehyde (0.0145 g, 0.107 mmol), 3,4,5-tri(tetradecyloxy)aniline (0.157 g, 0.215 mmol), and $MnCl_2 \cdot 4H_2O$ (0.0212 g, 0.107 mmol). Appearance: ochre solid (0.128 g, 71%); IR (KBr): $\tilde{\nu} = 1586\ cm^{-1}$ (C=N); FAB-MS: *m/z*: 1649 $[M-Cl]^+$; UV/Vis ($CHCl_3$): λ_{max} (ε) = 244 (2.4×10^4), 290 (8.2×10^3), 441 nm ($1.5 \times 10^4\ mol^{-1}\,dm^3\,cm^{-1}$); elemental analysis calcd (%) for for $C_{103}Cl_2H_{183}N_3O_6Mn$: C 73.40, H 10.94, N 2.49; found: C 73.52, H 11.03, N 2.55.

[$MnCl_2(L^{16})$]: This complex was prepared from pyridinedicarboxaldehyde (0.0138 g, 0.102 mmol), 3,4,5-tri(hexadecyloxy)aniline (0.166 g, 0.204 mmol), and $MnCl_2 \cdot 4H_2O$ (0.0202 g, 0.102 mmol). Appearance: yellow-ochre needles (0.164 g, 87%); IR (KBr): $\tilde{\nu} = 1585\ cm^{-1}$ (C=N); FAB-MS: *m/z*: 1818 $[M-Cl]^+$; UV/Vis ($CHCl_3$): λ_{max} (ε) = 247 (2.5×10^4), 295 (8.0×10^3), 441 nm ($1.7 \times 10^4\ mol^{-1}\,dm^3\,cm^{-1}$); elemental analysis calcd (%) for $C_{115}Cl_2H_{207}N_3O_6Mn$: C 74.51, H 11.26, N 2.27; found: C 74.90, H 11.56, N 2.48; conductivity ($CHCl_3$): $\Lambda = 0\ S\,m^{-2}\,mol^{-1}$.

[$ZnCl_2(L^1)$]: A solution of 2,6-pyridinedicarboxaldehyde (0.0150 g, 0.111 mmol) and 3,4,5-tri(methoxy)aniline (0.0407 g, 0.222 mmol) in $CHCl_3$ (70 mL) was stirred at room temperature for 10 min, the color changing to yellow. A solution of $ZnCl_2$ (0.0151 g, 0.111 mmol) in EtOH (7.5 mL) was added and this mixture was heated at reflux for 21 h. The yellow crystalline precipitate which formed upon cooling was collected by filtration and washed with little cold EtOH, with a yield of 0.0641 g (96%). ^1H NMR (300.13 MHz, CD_3CN): $\delta = 8.92$ (s, 1H; *H*C=N), 8.48 (t, $^3J(H,H) = 7.8$ Hz, 1H; Py-H_{para}), 8.15 (d, $^3J(H,H) = 7.8$ Hz, 2H; Py-H_{meta}), 7.39 (s, 4H; Ar-*H*), 3.89 (s, 12H; *m*-OCH_3), 3.73 ppm (s, 6H; *p*-OCH_3); IR (KBr): $\tilde{\nu} = 1589$ (m; C=N), 1125 cm^{-1} (vs; C–O); FAB-MS: *m/z*: 566 $[M-Cl]^+$, 603 $[M]^+$; elemental analysis calcd (%) for $C_{25}Cl_2H_{27}N_3O_6Zn$: C 49.90, H 4.52, N 6.98; found: C 50.10, H 4.51, N 6.79. X-ray quality crystals of the product were grown by layering L^1 (0.0101 g, 0.0217 mmol) in benzonitrile (1.5 mL) and $ZnCl_2$ (0.0030 g, 0.0220 mmol) in EtOH (1.5 mL) over one week, to give orange columns.

[$ZnCl_2(L^8)$]: A solution of 2,6-pyridinedicarboxaldehyde (0.0104 g, 0.0770 mmol) and 3,4,5-tri(octyloxy)aniline (0.0735 g, 0.154 mmol) in $CHCl_3$ (20 mL) was stirred at room temperature for 10 min, before adding a solution of $ZnCl_2$ (0.0105 g, 0.0770 mmol) in EtOH (7.5 mL). The deep yellow reaction mixture was heated under reflux for 20 h and then left to evaporate at room temperature for 3 days, after which time the product precipitated as yellow needles, isolated by filtration and washed with a small amount of cold EtOH, in 92% yield (0.0847 g). ^1H NMR (300.13 MHz, $CDCl_3$): $\delta = 8.81$ (s, 2H; HC=N), 7.94 (t, $^3J(H,H) = 7.5$ Hz, 1H; Py-H_4), 7.70 (d, $^3J(H,H) = 7.5$ Hz, 2H; Py-$H_{3/5}$), 7.26 (s, 4H; Ar-*H*), 4.03 (t, $^3J(H,H) = 6.3$ Hz, 8H; *m*-OCH_2), 3.95 (t, $^3J(H,H) = 6.6$ Hz, 4H; *p*-OCH_2), 1.82–1.29 (m, 72H; CH_2), 0.88 ppm (2 overlapping triplets, 18H; CH_3); ^{13}C NMR (75.48 MHz, $CDCl_3$): $\delta = 152.97$ (C_q), 150.14 (HC=N), 147.87 (C_q), 141.92 (Py-C_4), 139.51 (C_q), 128.36 (Py-$C_{3/5}$), 102.69 (Ar-C_2), 73.56 (*p*-OCH_2), 69.24 (*m*-OCH_2), 31.95, 30.37, 29.61, 29.56, 29.42, 26.22, 26.11, 22.76 (CH_2), 14.16 (CH_3); IR (KBr): $\tilde{\nu} = 1586\ cm^{-1}$ (C=N); FAB-MS: *m/z*: 1116 $[M-2Cl]^+$, 1153 $[M-Cl]^+$; UV/Vis ($CHCl_3$): λ_{max} (ε) = 244 (3.3×10^4), 286 (1.5×10^4), 441 nm ($2.2 \times 10^4\ mol^{-1}\,dm^3\,cm^{-1}$). The microanalysis gives satisfactory results with three molecules of water. Elemental analysis calcd (%) for $C_{67}Cl_2H_{111}N_3O_6Zn \cdot 3H_2O$: C 64.64, H 9.47, N 3.38; found: C 64.70, H 9.24, N 3.24.

[$ZnCl_2(L^{10})$]: This complex was prepared from pyridinedicarboxaldehyde (0.0117 g, 0.0866 mmol), 3,4,5-tri(decyloxy)aniline (0.0973 g, 0.173 mmol), and $ZnCl_2$ (0.0118 g, 0.0866 mmol). Appearance: crystalline orange solid (0.101 g, 84%); ^1H NMR (300.13 MHz, $CDCl_3$): $\delta = 8.83$ (s, 2H; HCM=N), 7.92 (t, $^3J(H,H) = 7.5$ Hz, 1H; Py-H_4), 7.68 (d, $^3J(H,H) = 7.5$ Hz, 2H; Py-$H_{3/5}$), 7.26 (s, 4H; Ar-*H*), 4.03 (t, $^3J(H,H) = 6.3$ Hz, 8H; *m*-OCH_2), 3.95 (t, $^3J(H,H) = 6.6$ Hz, 4H; *p*-OCH_2), 1.81–1.28 (m, 96H; CH_2), 0.88 ppm (2 overlapping triplets, 18H; CH_3); ^{13}C NMR (75.48 MHz, $CDCl_3$): $\delta = 153.01$ (C_q), 149.94 (HC=N), 148.00 (C_q), 142.02 (Py-C_4), 139.67 (C_q), 128.25 (Py-$C_{3/5}$), 102.58 (Ar-C_2), 73.53 (*p*-OCH_2), 69.20 (*m*-OCH_2), 31.95, 30.32, 29.70, 29.55, 29.41, 26.17, 26.07, 22.70 (CH_2), 14.10 (CH_3); IR (KBr): $\tilde{\nu} = 1587\ cm^{-1}$ (C=N); FAB-MS: *m/z*: 1322 $[M-Cl]^+$; UV/Vis ($CHCl_3$): λ_{max} (ε) = 246 (3.7×10^4), 296 (1.4×10^4), 440 ($3.0 \times 10^4\ mol^{-1}\,dm^3\,cm^{-1}$). The microanalysis gives satisfactory results with two molecules of water. Elemental analysis calcd (%) for $C_{79}Cl_2H_{135}N_3O_6Zn \cdot 2H_2O$: C 68.11, H 10.06, N 3.02; found: C 67.96, H 10.08, N 2.90.

[$ZnCl_2(L^{12})$]: This complex was prepared from pyridinedicarboxaldehyde (0.0111 g, 0.0821 mmol), 3,4,5-tri(dodecyloxy)aniline (0.106 g, 0.164 mmol), and $ZnCl_2$ (0.0112 g, 0.0822 mmol). Appearance: yellow solid (0.104 g, 81%); ^1H NMR (300.13 MHz, $CDCl_3$): $\delta = 8.84$ (s, 2H; HC=N), 7.91 (t, $^3J(H,H) = 7.7$ Hz, 1H; Py-H_4), 7.68 (d, $^3J(H,H) = 7.7$ Hz,

2H; Py-$H_{3/5}$), 7.26 (s, 4H; Ar-H), 4.02 (t, ^3J(H,H) = 6.3 Hz, 8H; m-OCH_2), 3.95 (t, ^3J(H,H) = 6.3 Hz, 4H; p-OCH_2), 1.81–1.27 (m, 120H; CH_2), 0.88 ppm (2 overlapping triplets, 18H; CH_3); ^{13}C NMR (75.48 MHz, $CDCl_3$): δ = 152.99 (C_q), 150.11 (C_q), 147.91 (HC=N), 142.35 (Py-C_4), 139.52 (C_q), 128.34 (Py-$C_{3/5}$), 102.69 (Ar-C_2), 73.57 (central OCH$_2$), 69.25 (lateral OCH$_2$), 32.03, 30.40, 29.83, 29.66, 29.48, 26.25, 26.16, 22.77 (CH$_2$), 14.17 ppm (CH$_3$); IR (KBr): $\tilde{\nu}$ = 1587 cm^{-1} (C=N); FAB-MS: m/z: 1491 [M − Cl]$^+$; UV/Vis ($CHCl_3$): λ_{max} (ε) = 244 (2.7×10^4), 293 (1.1×10^4), 440 nm (2.0×10^4 mol^{-1} dm^3 cm^{-1}); elemental analysis calcd (%) for $C_{91}Cl_2H_{159}N_3O_6Zn$: C 71.55, H 10.49, N 2.75; found: C 72.26, H 10.58, N 2.45.

[ZnCl$_2$(L^{14})]: This complex was prepared from pyridinedicarboxaldehyde (0.0123 g, 0.091 mmol), 3,4,5-tri(tetradecyloxy)aniline (0.133 g, 0.182 mmol), and $ZnCl_2$ (0.0124 g, 0.091 mmol). Appearance: crystalline yellow solid (0.119 g, 77%); ^{1}H NMR (300.13 MHz, $CDCl_3$): δ = 8.77 (s, 2H; HC=N), 8.04 (t, ^3J(H,H) = 7.5 Hz, 1H; Py-H_4), 7.76 (*d*, ^3J(H,H) = 7.5 Hz, 2H; Py-$H_{3/5}$), 7.29 (*s*, 4H; Ar-H), 4.05 (*t*, ^3J(H,H) = 6.2 Hz, 8H; m-OCH_2), 3.97 (t, ^3J(H,H) = 6.6 Hz, 4H; p-OCH_2), 1.82–1.27 (m, 144H; CH_2), 0.88 ppm (2 overlapping triplets, 18H; CH_3); ^{13}C NMR (75.48 MHz, $CDCl_3$): δ = 153.18 (C_q), 149.84 (C_q), 148.26 (HC=N), 142.32 (Py-C_4), 139.91 (C_q), 128.26 (Py-$C_{3/5}$), 102.63 (Ar-C_2), 73.62 (p-OCH$_2$), 69.31 (m-OCH$_2$), 32.01, 31.41, 29.84, 29.63, 29.45, 26.25, 26.16, 22.76 (CH$_2$), 14.17 ppm (CH$_3$); IR (KBr): $\tilde{\nu}$ = 1588 cm^{-1} (C=N); FAB-MS: m/z: 1657 [M − 2Cl]$^+$; UV/Vis ($CHCl_3$): λ_{max} (ε) = 242 (2.5×10^4), 296 (8.5×10^3), 440 nm (2.0×10^4 mol^{-1} dm^3 cm^{-1}); elemental analysis calcd (%) for $C_{103}Cl_2H_{183}N_3O_6Zn$: C 72.94, H 10.88, N 2.48; found: C 73.04, H 11.00, N 2.30.

[ZnCl$_2$(L^{16})]: This complex was prepared from pyridinedicarboxaldehyde (0.012 g, 0.0888 mmol), 3,4,5-tri(hexadecyloxy)aniline (0.145 g, 0.178 mmol), and $ZnCl_2$ (0.0121 g, 0.0888 mmol). Appearance: crystalline yellow solid (0.134 g, 81%). ^{1}H and ^{13}C NMR give the same spectrum as for [$ZnCl_2$(L^8)] except for the integration of the aliphatic part, due to the incremental increase of the chain-length. ^{1}H NMR (300.13 MHz, $CDCl_3$): δ = 8.82 (s, 2H; HC=N), 7.93 (t, ^3J(H,H) = 7.8 Hz, 1H; Py-H_4), 7.69 (d, ^3J(H,H) = 7.8 Hz, 2H; Py-$H_{3/5}$), 7.26 (s, 4H; Ar-H), 4.03 (t, ^3J(H,H) = 6.3 Hz, 8H; m-OCH_2), 3.95 (t, ^3J(H,H) = 6.6 Hz, 4H; p-OCH_2), 1.81–1.26 (m, 168H; CH_2), 0.88 ppm (2 overlapping triplets, 18H; CH_3); ^{13}C NMR (75.48 MHz, $CDCl_3$): δ = 153.17 (C_q), 149.84 (C_q), 148.25 (HC=N), 142.17 (Py-C_4), 139.87 (C_q), 128.25 (Py-$C_{3/5}$), 102.70 (Ar-C_2), 73.61 (p-OCH$_2$), 69.33 (m-OCH$_2$), 31.99, 30.42, 29.82, 29.63, 29.44, 26.25, 26.17, 22.74 (CH$_2$), 14.14 ppm (CH$_3$); IR (KBr): $\tilde{\nu}$ = 1586 cm^{-1} (C=N); FAB-MS: m/z: 1827 [M − Cl]$^+$; UV/Vis ($CHCl_3$): λ_{max} (ε) = 246 (2.6×10^4), 291 (9.5×10^3), 440 nm (2.0×10^4 mol^{-1} dm^3 cm^{-1}); elemental analysis calcd (%) for $C_{115}Cl_2H_{207}N_3O_6Zn$: C 74.09, H 11.19, N 2.25; found: C 74.38, H 11.16, N 2.49; conductivity ($CHCl_3$): Λ = 0 S m^{-2} mol^{-1}.

[CoCl$_2$(L^8)]: A solution of 2,6-pyridinedicarboxaldehyde (0.0104 g, 0.0770 mmol) and 3,4,5-tri(octyloxy)aniline (0.0735 g, 0.154 mmol) in $CHCl_3$ (20 mL) was stirred at room temperature for 10 min, before adding a solution of $CoCl_2$ (0.0100 g, 0.0770 mmol) in EtOH (7.5 mL). The brown-red reaction mixture was heated under reflux for 20 h and then left to evaporate at room temperature for 3 days, after which the product precipitated as brown needles, isolated by filtration and washed with a small amount of cold EtOH, in 70% yield (0.0638 g). IR (KBr): $\tilde{\nu}$ = 1589 cm^{-1} (C=N); FAB-MS: m/z: 1113 [M − 2Cl]$^+$, 1148 [M − Cl]$^+$; UV/Vis ($CHCl_3$): λ_{max} (ε) = 244 (2.5×10^4), 299 (9.0×10^3), 408 nm (1.7×10^4 6mol^{-1} dm^3 cm^{-1}). The microanalysis gives satisfactory results with one molecule of water. Elemental analysis calcd (%) for $C_{67}Cl_2H_{111}N_3O_6Co \cdot 1H_2O$: C 66.93, H 9.47, N 3.49; found: C 66.36, H 9.32, N 3.23.

[CoCl$_2$(L^{10})]: This complex was prepared from pyridinedicarboxaldehyde (0.0118 g, 0.0873 mmol), 3,4,5-tri(decyloxy)aniline (0.0981 g, 0.175 mmol), and $CoCl_2$ (0.0113 g, 0.087 mmol). Appearance: crystalline dark brown solid (0.075 g, 63%); IR (KBr): $\tilde{\nu}$ = 1587 cm^{-1} (C=N); FAB-MS: m/z: 1280 [M − 2Cl]$^+$, 1317 [M − Cl]$^+$; UV/Vis ($CHCl_3$): λ_{max} (ε) = 246 (2.3×10^4), 300 (8.6×10^3), 411 nm (1.2×10^4 mol^{-1} dm^3 cm^{-1}). The microanalysis gives satisfactory results with one molecule of water. Elemental analysis calcd (%) for $C_{79}Cl_2H_{135}N_3O_6Co \cdot 1H_2O$: C 68.32, H 10.09, N 3.03; found: C 68.12, H 10.04, N 2.81.

[CoCl$_2$(L^{12})]: This complex was prepared from pyridinedicarboxaldehyde (0.0115 g, 0.0851 mmol), 3,4,5-tri(dodecyloxy)aniline (0.11 g, 0.17 mmol), and $CoCl_2$ (0.0111 g, 0.0855 mmol). Appearance: brown needles (0.093 g, 71%); IR (KBr): $\tilde{\nu}$ = 1588 cm^{-1} (C=N); FAB-MS: m/z: 1449 [M − 2Cl]$^+$, 1485 [M − Cl]$^+$; UV/Vis ($CHCl_3$): λ_{max} (ε) = 244 (2.5×10^4), 286 (8.2×10^3), 298 (7.8×10^3), 410 nm (1.3×10^4 mol^{-1} dm^3 cm^{-1}). The microanalysis gives satisfactory results with one molecule of water. Elemental analysis calcd (%) for $C_{91}Cl_2H_{159}N_3O_6Co \cdot 1H_2O$: C 71.02, H 10.41, N 2.73; found: C 70.85, H 10.44, N 2.63.

[CoCl$_2$(L^{14})]: This complex was prepared from pyridinedicarboxaldehyde (0.0109 g, 0.0807 mmol), 3,4,5-tri(tetradecyloxy)aniline (0.118 g, 0.162 mmol), and $CoCl_2$ (0.0105 g, 0.0809 mmol). Appearance: brown solid (0.91 g, 65%); IR (KBr): $\tilde{\nu}$ = 1585 cm^{-1} (C=N); FAB-MS: m/z: 1617 [M − 2Cl]$^+$, 1652 [M − Cl]$^+$; UV/Vis ($CHCl_3$): λ_{max} (ε) = 246 (2.7×10^4), 300 (8.5×10^3), 406 nm (1.4×10^4 mol^{-1} dm^3 cm^{-1}). The microanalysis gives satisfactory results with three molecules of water. Elemental analysis calcd (%) for $C_{103}Cl_2H_{183}N_3O_6Co \cdot 3H_2O$: C 70.96, H 10.93, N 2.41; found: C 70.32, H 10.91, N 2.47.

[CoCl$_2$(L^{16})]: This complex was prepared from pyridinedicarboxaldehyde (0.011 g, 0.0814 mmol), 3,4,5-tri(hexadecyloxy)aniline (0.133 g, 0.163 mmol), and $CoCl_2$ (0.0106 g, 0.0816 mmol). Appearance: crystalline dark brown solid (0.14 g, 90%); IR (KBr): $\tilde{\nu}$ = 1585 cm^{-1} (C=N); FAB-MS: m/z: 1785 [M − 2Cl]$^+$, 1821 [M − Cl]$^+$; UV/Vis ($CHCl_3$): λ_{max} (ε) = 247 (2.6×10^4), 301 (8.0×10^3), 415 nm (1.5×10^4 mol^{-1} dm^3 cm^{-1}). The microanalysis gives satisfactory results with three molecules of water. Elemental analysis calcd (%) for $C_{115}Cl_2H_{207}N_3O_6Co \cdot 3H_2O$: C 72.25, H 11.23, N 2.20; found: C 72.01, H 11.00, N 2.23; conductivity ($CHCl_3$): Λ = 0 S m^{-2} mol^{-1}.

Acknowledgement

We thank the EPSRC (UK), NEDO (Japan), and the University of Nottingham for financial support. We also thank the EPSRC Mass Spectrometry service (University of Swansea). B.D. thanks Dr Benoît Heinrich for his skills and technical assistance for the dilatometry experiment.

[1] a) *Metallomesogens, Synthesis, Properties and Applications* (Ed.: J. L. Serrano), VCH, Weinheim, **1996**; b) F. Neve, *Adv. Mater.* **1996**, *8*, 277–289; c) B. Donnio, D. W. Bruce, *Struct. Bonding* **1999**, *95*, 193–247; d) S. R. Collinson, D. W. Bruce in *Transition Metals in Supramolecular Chemistry* (Ed.: J. P. Sauvage), Wiley, New York, **1999**, Chapter 7, pp. 285–369.

[2] a) L. Ziminski, J. Malthête, *J. Chem. Soc. Chem. Commun.* **1990**, 1495–1496; b) Y. Galyametdinov, G. Ivanova, K. Griesar, A. Prosvirin, I. Ovchinnikov, W. Haase, *Adv. Mater.* **1992**, *4*, 739–741; c) F. Neve, M. Ghedini, *J. Inclusion Phenom. Mol. Recognit. Chem.* **1993**, *15*, 259–272; d) H. Zheng, T. M. Swager, *J. Am. Chem. Soc.* **1994**, *116*, 761–762; e) R. Deschenaux, I. Kosztics, B. Nicolet, *J. Mater. Chem.* **1995**, *5*, 2291–2295; f) S. Morrone, D. Guillon, D. W. Bruce, *Inorg. Chem.* **1996**, *35*, 7041–7048; g) U. Stebani, G. Lattermann, M. Wittenbger, J. H. Wendorff, *Angew. Chem.* **1996**, *108*, 1941–1943; *Angew. Chem. Int. Ed. Engl.* **1996**, *35*, 1858–1861; h) R. Deschenaux, B. Donnio, G. Rheinwald, F. Stauffer, G. Süss-Fink, J. Velker, *J. Chem. Soc. Dalton Trans.* **1997**, 4351–4355; i) X. H. Liu, I. Manners, D. W. Bruce, *J. Mater. Chem.* **1998**, *8*, 1555–1560; j) J. Barbera, A. Elduque, R. Gimenez, F. J. Lahoz, J. A. Lopez, L. A. Oro, J. L. Serrano, *Inorg. Chem.* **1998**, *37*, 2960–2967; k) S. T. Trzaska, H. F. Hsu, T. M. Swager, *J. Am. Chem. Soc.* **1999**, *121*, 4518–4519; l) S. T. Trzaska, H. Zheng, T. M. Swager, *Chem. Mater.* **1999**, *11*, 130–134; m) J. Szydlowska, A. Krowczynski, E. Gorecka, D. Pociecha, *Inorg. Chem.* **2000**, *39*, 4879–4885; n) K. Binnemans, Y. G. Galyametdinov, R. Van Deun, D. W. Bruce, S. R. Collinson, A. P. Polishchuk, I. Bikchantaev, W. Haase, A. W. Prosvirin, L. Tinchurina, I. Litvinov, A. Gubajdullin, A. Rakhmatullin, K. Uytterhoeven, L. Van Meervelt, *J. Am. Chem. Soc.* **2000**, *122*, 4335–4344; o) R. Ziessel, L. Douce, A. El-ghayoury, A. Harriman, A. Skoulios, *Angew. Chem.* **2000**, *112*, 1549–1553; *Angew. Chem. Int. Ed. Engl.* **2000**, *39*, 1489–1493; p) M. Ghedini, D. Pucci, A. Crispini, G. Barberio, *Organometallics* **1999**, *18*, 2116–2124; q) Yu. Galyametdinov, V. Ksenofontov, A. Prosvirin, I. Ovchinnikov, G. Ivanova, P. Gütlich, W. Haase, *Angew. Chem.* **2001**, *113*, 4399–4401; *Angew. Chem. Int. Ed. Engl.* **2001**, *40*, 4269–4271; r) K.

Binnemans, K. Lodewyckx, B. Donnio, D. Guillon, *Chem. Eur. J.* **2002**, *8*, 1101–1105.
[3] a) J. Barbera in ref [1a], Chapter 4; b) M. B. Ros in ref. [1a], Chapter 11.
[4] R. Atencio, J. Barbera, C. Cativiela, F. J. Lahoz, J. L. Serrano, A. M. Zurbano, *J. Am. Chem. Soc.* **1994**, *116*, 11558–11559.
[5] a) C. K. Lai, A. G. Serrete, T. M. Swager, *J. Am. Chem. Soc.* **1992**, *114*, 7948–7949; b) A. G. Serrete, T. M. Swager, *J. Am. Chem. Soc.* **1993**, *115*, 8879–8880.
[6] a) H. Zheng, C. K. Lai, T. M. Swager, *Chem. Mater.* **1994**, *6*, 101–103; b) S. T. Trzaska, T. M. Swager, *Chem. Mater.* **1998**, *10*, 438–443.
[7] a) C. K. Lai, Y. S. Pang, C. H. Tsai, *J. Mater. Chem.* **1998**, *8*, 2605–2610; b) C. D. Yang, Y. S. Pang, C. K. Lai, *Liq. Cryst.* **2001**, *28*, 191–195.
[8] S. Coco, P. Espinet, J. M. Martin-Alvarez, A. M. Levelut, *J. Mater. Chem.* **1997**, *7*, 19–23.
[9] S. Coco, F. Diez-Exposito, P. Espinet, C. Fernandez-Mayordomo, J. M. Martin-Alvarez, A. M. Levelut, *Chem. Mater.* **1996**, *10*, 3666–3671.
[10] A. G. Serrete, C. K. Lai, T. M. Swager, *Chem. Mater.* **1994**, *6*, 2252–2268.
[11] N. Hoshino, *Coord. Chem. Rev.* **1998**, *174*, 77–100.
[12] a) E. C. Alyea, G. Ferguson, R. J. Restivo, *Inorg. Chem.* **1975**, *14*, 2491–2495 and references therein; b) A. J. Blake, A. J. Lavery, T. I. Hyde, M. Schröder, *J. Chem. Soc. Dalton Trans.* **1989**, 965–970.
[13] a) E. C. Alyea, G. Ferguson, R. J. Restivo P. H. Merrell, *J. Chem. Soc. Chem. Commun.* **1975**, *8*, 269–270; b) E. C. Alyea, P. H. Merrell, *Inorg. Chim. Acta* **1978**, *28*, 91–97; c) G. Ferguson, R. J. Restivo, *J. Chem. Soc. Dalton Trans.* **1976**, 518–521; d) D. A. Edwards, M. F. Mahon, W. R. Martin, K. C. Molloy, P. E. Fanwick, R. A. Walton, *J. Chem. Soc. Dalton Trans.* **1990**, 3161–3168; e) D. A. Edwards, S. D. Edwards, W. R. Martin, T. J. Pringle, P. Thornton, *Polyhedron* **1992**, *11*, 1569–1573; f) A. J. Blake, A. J. Lavery, M. Schröder, *Acta Crystallogr. Sect. C* **1996**, *52*, 37–39.
[14] a) B. L. Small, M. Brookhart, A. M. A. Bennett, *J. Am. Chem. Soc.* **1998**, *120*, 4049–4050; b) E. A. H. Griffiths, G. J. P. Britovsek, V. C. Gibson, I. R. Gould, *Chem. Commun.* **1999**, 1333–1334; c) G. J. P. Britovsek, M. Bruce, V. C. Gibson, B. S. Kimberley, P. J. Maddox, S. Mastroianni, S. J. McTavish, C. Redshaw, G. A. Solan, S. Strömberg, A. J. P. White, D. J. Williams, *J. Am. Chem. Soc.* **1999**, *121*, 8728–8740 and references therein; d) B. de Bruin, E. Bill, E. Bothe, T. Weyhermüller, K. Wieghardt, *Inorg. Chem.* **2000**, *39*, 2936–2947.
[15] L. V. Andrew, N. W. Alcock, J. A. Heppert, D. H. Busch, *Inorg. Chem.* **1998**, *37*, 6912–6920 and references therein.
[16] P. Battistini, M. Carcelli, E. Dalcanale, C. Pelizzi, G. Pelizzi, L. Righini, *Mol. Cryst. Liq. Cryst.* **1998**, *309*, 167–188.
[17] L. Douce, R. Ziessel, *Mol. Cryst. Liq. Cryst.* **2001**, *362*, 133–145.
[18] L. Douce, A. El-ghayoury, A. Skoulios, R. Ziessel, *Chem. Commun.* **1999**, 2033–2034.
[19] A. Zinsou, M. Veber, H. Strzelecka, C. Jallabert, P. Fourré, *New. J. Chem.* **1993**, *17*, 309–313.
[20] G. J. P. Britovsek, V. C. Gibson, B. S. Kimberley, P. J. Maddox, S. J. McTavish, G. A. Solan, A. J. P. White, D. J. Williams, *Chem. Commun.* **1998**, 849–850.
[21] G. J. P. Britovsek, S. Mastroianni, G. A. Solan, S. P. D. Baugh, C. Redshaw, V. C. Gibson, A. J. P. White, D. J. Williams, M. R. J. Elsegood, *Chem. Eur. J.* **2000**, *6*, 2221–2231.
[22] A. M. Levelut, *J. Chim. Phys. Phys.-Chim. Biol.* **1983**, *80*, 149–161.
[23] D. Guillon, *Struct. Bonding* **1999**, *95*, 41–82.
[24] a) A. Skoulios, D. Guillon, *Mol. Cryst. Liq. Cryst.* **1988**, *165*, 317–332; b) C. Tschierske, *J. Mater. Chem.* **1998**, *8*, 1485–1508; c) C. Tschierske, *J. Mater. Chem.* **2001**, *11*, 2647–2671; d) C. Tschierske, *Annu. Rep. Prog. Chem. Sect. C* **2001**, *97*, 191–267.
[25] In the mesomorphic range, V_{mol} (Å^3) varies linearly with T. $V_{mol} = 3107.4 + 2.4050T$; ($V_{mol} = 3127.1 + 2.0617\,T + 0.001362\,T^2$).
[26] A. K. Doolittle, *J. Appl. Phys.* **1951**, *22*, 1471–1475. Volume of six aliphatic chains of 16 carbon atoms: see ref. [31].
[27] $V_{Ar} = 415$ Å^3.
[28] V_{mol} (Å^3) in Col$_r$ ($T < 105\,^\circ$C): $V_{mol} = 3117.04 + 2.3\,T$; V_{mol} in Col$_h$ ($T > 105\,^\circ$C): $V_{mol} = 3098.15 + 2.46\,T$.
[29] M. Marcos, R. Jiménez, J. L. Serrano, B. Donnio, B. Heinrich, D. Guillon, *Chem. Eur. J.* **2001**, *7*, 1006–1013.
[30] $V_{Ar} = 414.35 + 0.01T - 1.15 \times 10^{-3}T^2$.
[31] V_{mol} can be written as a sum of elementary volumes associated to the different segments of the molecule according to $V_{mol} = V_{Ar} + V_{ch}$, whereby V_{Ar} and V_{ch} are the volumes of the aromatic rigid part and the aliphatic chains respectively. The molecular volume was obtained experimentally by a dilatometry experiment. V_{ch} was calculated as follows (all elementary volumes in Å^3 and T in $^\circ$C): $V_{ch} = 6nV_{CH_2} + 6\Delta V_{CH_3}$, where $V_{CH_2} = 26.5616 + 0.02023\,T$ is the volume of one methylene group and $\Delta V_{CH_3} = 27.14 + 0.01713\,T + 0.0004181\,T^2$ represents the volume difference between the terminal methyl group and a methylene group.
[32] $S = s_h = \frac{2}{\sqrt{3}} d_{10}^2$.
[33] $A = \sqrt{\frac{2}{\frac{1}{d_{11}^2} + \frac{1}{d_{1\bar{1}}^2} - \frac{1}{2d_{20}^2}}}$; $a = \frac{2d_{20}}{\sin\gamma}$; $b = \frac{A}{\sin\gamma}$;
$s_r = ab$ with $\gamma = \pi/2$; $s_o = ab$ with $\gamma \neq \pi/2$.
[34] SMART Area-Detector Software Package, Version 5.054, Bruker AXS, Madison, Wisconsin (USA), **1998**.
[35] J. Cosier, A. M. Glazer, *J. Appl. Crystallogr.* **1986**, *19*, 105–107.
[36] SAINT Frame Integration Software, Version 6.02a, Bruker AXS, Madison, Wisconsin (USA), **2000**.
[37] SADABS, Program for Applying Absorption Corrections to Area Detector Data, Bruker AXS, Madison, Wisconsin (USA), **1996**.
[38] G. M. Sheldrick, SHELXS-97, Program for Crystal Structure Solution, University of Göttingen, Göttingen (Germany), **1997**.
[39] G. M. Sheldrick, SHELXL-97, Program for Crystal Structure Refinement, University of Göttingen, Göttingen (Germany), **1997**.

Received: November 15, 2002 [F4578]

